MASSACHUSETTS INSTITUTE OF TECHNOLOGY VLSI PUBLICATIONS

VLSI Memo No. 89-517
March 1989

Comparison of Equipment Modeling Methods as Applied to the LPCVD of In-Situ P-Doped Polysilicon

Parmeet Singh Chaddha

Abstract

The orthogonal array design of experiments for process and equipment optimization is combined with a semi-empirical modelling approach based on dimensional analysis. This methodology is applied to *In-Situ* Phosphorus Doped Polysilicon Process via LPCVD. Taguchi's method of pure empiricism works well for the optimization of four different responses - thickness uniformity across the wafer, uniformity in a batch, growth rate, and the film resistivity for the process under consideration. The average thickness uniformity for the batch is optimized to 2.5% standard deviation. In separate confirmation runs a growth rate of 98 Å/min. and a resistivity of 1.25 mohm-cm are achieved. However, the dependence of Taguchi's method on the assumption that the process is free of parameter interactions distorts the prediction of nominal-is-the-best signal-to-noise ratio for the film thickness uniformity across the wafer. As a solution to such problems of purely experimental approach a thirteen terms semi-empirical model based on dimensional analysis is evolved for the film thickness uniformity in the process under consideration by using stepwise regression.

The average percent error in dimensional analysis model is about a third and the F-test is on the average six to seven times better than that for the corresponding primitive variables model. Dimensional analysis model predicts more reliably because the confidence intervals of its predictions are seen to be more than three times narrower than that for primitive variables model predictions. Also, the dimensional analysis model overcomes the problem encountered by Taguchi's method with regards to the importance of the process parameter interactions that the later tends to neglect.

Acknowledgements

Submitted to the Department of Mechanical Engineering in March 1989 in partial fulfillment of the requirement for the Degree of Master of Science in Mechanical Engineering. This research was supported in part by the Defense Advanced Research Projects Agency under contract numbers MDA972-88-K-0008 and N00014-85-K-0213.

Author Information

Chaddha: c/o Oracle Corporation, 2929 Campus Drive, Suite 100, San Mateo, CA 94403. (415) 598-8000.

COMPARISON OF EQUIPMENT MODELING METHODS AS APPLIED TO THE LPCVD OF *IN-SITU* P-DOPED POLYSILICON

by

Parmeet Singh Chaddha

SUBMITTED TO THE DEPARTMENT OF
MECAHNICAL ENGINEERING IN PARTIAL FULFILLMENT
OF THE DEGREE OF MASTER OF SCIENCE IN
MECHANICAL ENGINEERING

at the

MASSACHUSETTS INSTITUTE OF TECHNOLOGY

March, 1989

Signature of Author _____
Parmeet Singh Chaddha
Department of Mechanical Engineering
March 27, 1989

Certified by _____
Emanuel Sachs
Assistant Professor, Mechanical Engineering
Thesis Supervisor

Accepted by _____
Ain A. Sonin
Chairman, Graduate Committee

COMPARISON OF EQUIPMENT MODELING METHODS AS APPLIED TO THE LPCVD OF *IN-SITU* P-DOPED POLYSILICON

by

Parmeet Singh Chaddha

Submitted to the Department of Mechanical Engineering
on March 27, 1989 in partial fulfillment of the requirements
for the Degree of Master of Science in Mechanical Engineering.

Abstract

The orthogonal array design of experiments for process and equipment optimization is combined with a semi-empirical modelling approach based on dimensional analysis. This methodology is applied to *In-Situ* Phosphorus Doped Polysilicon Process via LPCVD. Taguchi's method of pure empiricism works well for the optimization of four different responses - thickness uniformity across the wafer, uniformity in a batch, growth rate, and the film resistivity for the process under consideration. The average thickness uniformity for the batch is optimized to 2.5% standard deviation. In separate confirmation runs a growth rate of 98 A°/min. and a resistivity of 1.25 mohm-cm are achieved. However, the dependence of Taguchi's method on the assumption that the process is free of parameter interactions distorts the prediction of nominal-is-the-best signal-to-noise ratio for the film thickness uniformity across the wafer. As a solution to such problems of purely experimental approach a thirteen terms semi-empirical model based on dimensional analysis is evolved for the film thickness uniformity in the process under consideration by using stepwise regression.

The average percent error in dimensional analysis model is about a third and the F-test is on the average six to seven times better than that for the corresponding primitive variables model. Dimensional analysis model predicts more reliably because the confidence intervals of its predictions are seen to be more than three times narrower than that for primitive variables model predictions. Also, the dimensional analysis model overcomes the problem encountered by Taguchi's method with regards to the importance of the process parameter interactions that the later tends to neglect.

Thesis Supervisor: Dr. Emanuel Sachs
Title: Assistant Professor, Mechanical Engineering

Biography

Parmeet Singh Chaddha was born in Punjab, India in 1964. He received a Bachelor's Degree in Mechanical Engineering from Massachusetts Institute of Technology in June of 1987. Since then he has been enrolled at Massachusetts Institute of Technology as a candidate for the Master's of Science Degree in Mechanical Engineering. While at MIT, he has been involved as a Research Assistant with the Computer Aided Fabrication (CAF) Group developing modeling methodology for the LPCVD of in-situ doped polysilicon process.

Table of Contents

1. INTRODUCTION

It is possible to study a physical process or a product design in terms of either analytical models or empiricism. Analytical models give good extrapolation and physical understanding of the system even without access to the modelled process. However, this mechanistic approach requires extensive effort for evolving and solving the relevant equations, e.g. differential equations of fluid flow processes. These equations may get extremely complex even for a system of moderate complexity and still not capture the completely relevant physics of the system. On the other hand, the empirical approach gives good accuracy within the experimental domain but it usually requires a large investment in terms of equipment time and expense. Also, lack of access to the desired experimental environment, which includes process equipment, trained operators, and data acquisition and processing capabilities, may be a big constraint on empirical approach.

1.1 Motivation

In this work the strengths of empiricism and analyticity are combined for the purpose of equipment design. The approach to equipment design and optimization, as outlined below, poses a special challenge for the *In-situ* Phosphorus Doped Polysilicon Process via LPCVD because of the tradeoff between the responses of growth rate, film thickness uniformity, and resistivity for this process. As will be explained later, this transport-limited deposition process is very sensitive to the geometry of the furnace and related quartzware. Therefore, it is attempted to incorporate these geometrical factors of the LPCVD equipment along with process parameters into our semi-empirical model.

1.2 Current Work

A parallel design of experiments, based on the *Taguchi Method* of orthogonal arrays [15], is used for designing equipment operating under a wide range of conditions for the *In-situ* Phosphorus Doped Polysilicon Process via LPCVD. The equipment design is realized in two ways. Firstly, the data from a set of parallel experiments based on Taguchi's orthogonal array design are directly used to optimize the equipment. Even though Taguchi's method allows for process and equipment optimization by using a small number of experiments, this method makes an important physical assumption that most manufacturing processes are can be modelled by main effects and some selected interactions. In order to overcome this limitation of Taguchi's method a second approach is used in which the empirical knowledge acquired from a set of parallel experiments is combined with the partial physical understanding of the process. This approach is used to develop a semi-empirical or a *"Smart Response Surface"* model, based on dimensional analysis, for the ratio (known as *SN ratio*) of thickness nonuniformity (measured by standard deviation) to thickness mean of the doped polysilicon film. This model is tested to predict the optimum conditions for equipment operation. By comparing these two approaches the physical significance of the SN ratio and, hence, its utility is highlighted.

2. EXPERIMENTAL DESIGN

The primary goal of any experimental design is to explore and improve the widest possible domain of process operation or product design with a minimum experimental effort. Of the two methods of experimentation - parallel and sequential, *orthogonal array parallel design* of experiments was selected to achieve the goal outlined before.

The orthogonal array approach has been popularized by Japanese quality expert G. Taguchi [15]. His idea of parameter design to make the product design and the manufacturing processes robust to the uncontrollable variations is based on the objective of setting process or product parameters to values that minimize the average squared deviation of the response from its target value.

2.1 Orthogonal Array Experimentation

One of the objectives of this research effort was to design optimal equipment for the *in-situ* phosphorus doped polysilicon LPCVD process by exploring a large operating space for the process parameters. This operating space consisted of the following eight *factors* or process parameters (see Fig. 2.1):

- interwafer distance (**w**),
- % hole area on the cage ($\mathbf{A_c}$),
- deposition temperature ($\mathbf{T_d}$),
- deposition pressure (**P**),
- inter-injector distance ($\mathbf{I_x}$),
- total silane flow ($\mathbf{Q_s}$),
- phosphine flow through injector #1 ($\mathbf{Q_{p1}}$), and
- phosphine flow through injector #2 ($\mathbf{Q_{p2}}$) .

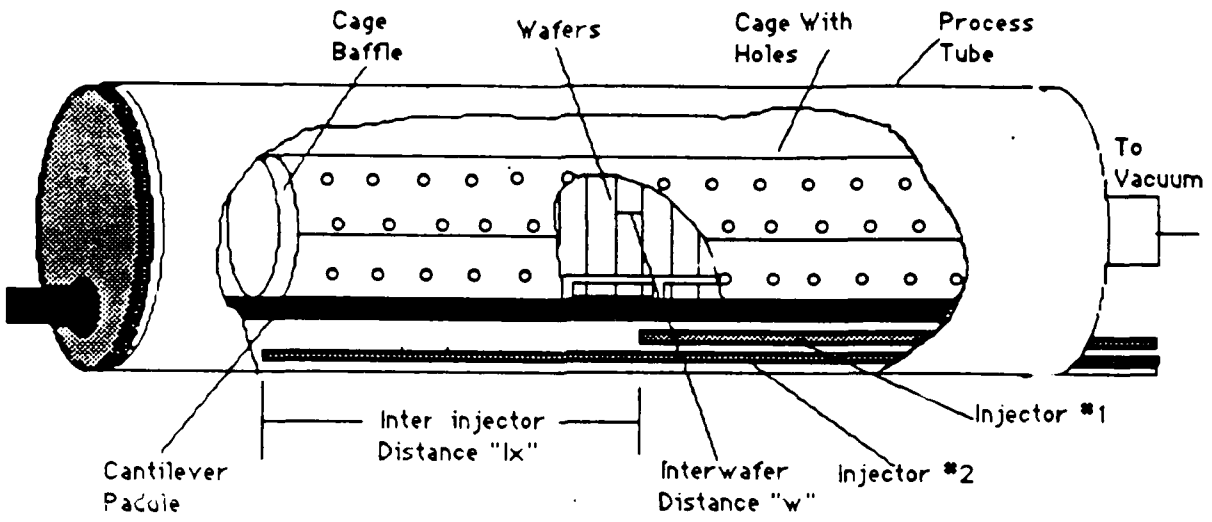

Fig.2.1: Schematic of LPCVD Process Tube

The effect of these process parameters was studied on the following three responses:

- film thickness uniformity,
- film growth rate and
- film resistivity.

The choice of eight process parameters was primarily made on the basis of the past work done on the *in-situ* doped polysilicon process [4, 5, 6, 7, 8, 9, 10]. The fact that eight parameters were selected to be used in an eight column L18 orthogonal array, imposed two limitations on the design:

- *the parameters had to be independent of each other* ; and
- *the factor interactions could not be studied from the results.*

As will be seen in the final results, these limitations were not severely inhibiting. Further, the semi-empirical model was evolved to overcome these limitations.

The settings or *levels* for these process parameters were chosen to span a wide but valid and useful operating space. The factors and their chosen levels are shown in Table 2.1 and the rationale for their selection is discussed in section 2.2. Besides covering a wide operating range, another consideration in designing the experiments was the constraint of time and expense. Therefore, only a partial factorial of the total number of possible combinations of the factor levels was considered for experiments. This partial factorial design was based on Taguchi L18 orthogonal array[1] as shown in Fig. 2.2. In

	W	A_c	T_d	P	I_x	Q_s	Q_{s1}	Q_{s2}
1)	1	1	1	1	1	1	1	1
2)	1	1	2	2	2	2	2	2
3)	1	1	3	3	3	3	3	3
4)	1	2	1	1	2	2	3	3
5)	1	2	2	2	3	3	1	1
6)	1	2	3	3	1	1	2	2
7)	1	3	1	2	1	3	2	3
8)	1	3	2	3	2	1	3	1
9)	1	3	3	1	3	2	1	2
10)	2	1	1	3	3	2	2	1
11)	2	1	2	1	1	3	3	2
12)	2	1	3	2	2	1	1	3
13)	2	2	1	2	3	1	3	2
14)	2	2	2	3	1	2	1	3
15)	2	2	3	1	2	3	2	1
16)	2	3	1	3	2	3	1	2
17)	2	3	2	1	3	1	2	3
18)	2	3	3	2	1	2	3	1

Fig. 2.2: Taguchi L18 Orthogonal Array[1]

[1] The columns of the array are mutually orthogonal in a combinatoric sense. For any pair of columns, all combinations of factor levels occur and they occur equal number of times. This balancing property of the columns implies *orthogonality*.

order to cover the full factorial of the factor level combinations one needs to do 2^1X3^7 = 4374 distinct experiments. However, an orthogonal array experiment design provides us with neccessary data with only 18 experiments, provided the superposition or additive model [17] for the main effects of the parameters holds for the process under scrutiny.

2.2 Process Parameter Levels

	Factor	Levels		
		1	2	3
1	Interwafer distance (W)	7.5 mm	15 mm	—
2	Percent Hole Area on Cage (A_c)	0.5 %	3.5%	20%
3	Deposition Temperature (T_d)	580°C	600°C	620°C
4	Pressure in the Tube (P)	325 mtorr	350 mtorr	375 mtorr
5	Inter-Injector Distance (l_x)	40.0 cm	52.5cm	65.0cm
6	Total Silane Flow Rate (Q_s)	250 sccm	300 sccm	350 sccm
7	Injector 1 Phosphine Flow Rate (Q_{P1})	0.6 sccm	1.6 sccm	4.2 sccm
8	Injector 2 Phosphine Flow Rate (Q_{P2})	26 sccm	0.7 sccm	1.8 sccm

Table 2.1: Process Parameter Levels

Table 2.1 shows the factor levels used in the experiments. A limited range of two levels, every slot in the boat (level 1) and every other

slot (level 2), was chosen for interwafer distance "w" because it was desired that the film properties be improved without cutting the load size drastically. Since "w" had only two levels, it was placed in column one of the orthogonal array in Fig 2.2[1]. The levels for % hole area "A_c" on the cage were chosen based on the past work done in the process lab at BTU Engineering. According to this work the film thickness uniformity deteriorated rapidly for effective cage hole area above 10%. A wide range of 0.5-20% "A_c" was selected and divided geometrically into three levels shown in Table 2.1. The number of levels were limited to three because the quartzware cost for the cages is high. Since changing the cage between experiments is time consuming, the process parameter "A_c" was placed in second column of the orthogonal array so that more experiments could be completed with the same cage setup. The levels for deposition temperature "T_d" were based on the fact that the *in-situ* doped silicon film via LPCVD is amorphous when deposited at temperature below 580°C and the film surface roughness deteriorates rapidly above 620°C. Although higher deposition temperature will enhance the growth rate of the film, the out-diffusion of the dopant molecules become very significant at higher temperatures thereby raising the film resistivity. Keeping in view the tradeoffs between film quality, growth rate and film resistivity, "T_d" levels of 580°C, 600°C and 620°C were chosen. The levels for deposition pressure "P" were determined by low pressure considerations for this LPCVD process and by the constraint imposed by the capacity of the vacuum pump used. The vacuum pump failed to pump pressures below 325 mtorr at the highest silane flow rate of 350 sccm. "I_x" levels were chosen based on the past work in the BTU Engineering process lab for controlling down-the-load film thickness unformity.

Flow rates for silane and phosphine through the two injectors were chosen based on the base line runs made in the past by the BTU Engineering staff. The ratio of the flows of either of these gases

[1] The entries "1", "2", "3" in the orthogonal array represent the levels of the process parameters. Row numbers 1-18 represent the run numbers.

through injector #1 to that through injector #2 was 2.2:1.0. The lower flow rates in injector #2 is explained by the fact that the role of the second injector is only to compensate for down-the-load depletion effects, if any. The total silane flow through the two injectors was considered as one parameter rather than two different injector flows because silylene, and not silane, is the dominant reactant in this transport limited process. Therefore, it is the total amount of silane flowing through two injectors and its homogeneous phase product silylene that is important and not the axial distribution of silane in the furnace. In any case the axial distribution of silane and the consequent down-the-load depletion effects are controlled by "I_x". Also, the coupling of two silane flows into one parameter reduced the number of process parameters to eight so that they could fit in a L18 orthogonal array. In contrast, the phosphine flow rates were independently controlled so that their distribution in two injectors could be independently controlled to influence across-the-wafer film thickness uniformity down the batch.

2.3 Noise Factors and Testing Conditions

Although the influence of the process parameters was studied by L18 experimental design, the influence of various random variations on the process demanded an extended approach of identifying various *noise factors* and studying their influence on the responses under consideration.

Some of the noise factors identified were: predeposition anneal, paddle off-center in the furnace, humidity, room temperature, wafer thickness variations, impurity atoms in the lattice, film growth on the tube liner, and measuring device limitations. Except for the predeposition anneal and paddle off-center, all other noise factors were not controllable. In order to study the influence of noises in the system, replicate run was made at the end of the L18 experiments. The average error variance introduced by the various noise factors (i.e. the difference between the replicate runs) was

much smaller than the main effects of the process parameters. It was concluded that the repeatablity of the process was not greatly affected by the noises in the system and, therefore, noise factors were not considered in the subsequent steps. The comparison of a replicate with original run #1 in L18 is shown in Fig.2.3.

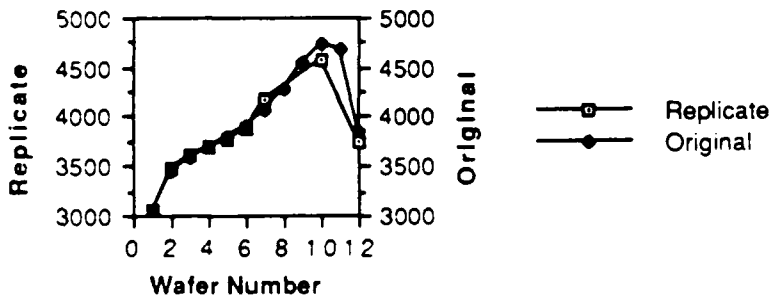

Fig. 2.3: Replicate vs Original for Run #1 in L18

2.4 Data Analysis Plan

The noise factors and random fluctuations in the process parameters vary the quality characterstic of a product from unit to unit within a batch. The average of squared deviation is called the *quadratic quality loss*. Such quadratic quality loss is expressed in dollar terms by multiplying the quality loss with a loss coefficient.

2.4.1 Cost Function

In order to optimize the thickness uniformity, growth rate and resistivity of the polysilicon film, a total cost function was derived that incorporated the quality loss due to inhomogeneous films, low growth rate and high resistivity. However, lack of data for *quality cost coefficients* (defined below) prevented us from calibrating the total cost function. Since these responses are in tradeoff with each other, their individual optimization was also done in order to compare their results and highlight the tradeoff.

Accordingly, the following loss functions were derived for the concerned responses (see Appendix B for derivation):

1) Thickness Uniformity Cost : Film thickness mean "$\mu_{T,i}$" and standard deviation "$\sigma_{T,i}$" was observed for each ith wafer in every batch. Based on these observations two different adjusted quality loss [14, 15, 17] functions were considered: across-the-wafer quality loss and overall loss in a batch. Considering nominal-the-best quadratic quality loss function, the total quality loss due to across-the-wafer thickness nonuniformity after the mean is adjusted to the target value is just the sum of losses due to individual wafers and is given by,

$$QL_{T1} = k_{T1}\,\mu_{T,t}^2\left[\frac{1}{n_w}\sum_{i=1}^{n_w}\left(\frac{\sigma_{T,i}^2}{\mu_{T,i}^2}\right)\right] \qquad (2.1)$$

where k_{T1} is the film thickness quality loss coefficient for a wafer, n_w is the number of wafers in the batch and $\mu_{T,t}$ is the target thickness. The corresponding signal-to-noise ratio SN_{T1}, as defined by G. Taguchi, is given by,

$$SN_{T1} = -10\log_{10}\left[\frac{1}{n_w}\sum_{i=1}^{n_w}\left(\frac{\sigma_{T,i}^2}{\mu_{T,i}^2}\right)\right] \qquad (2.2)$$

Note that the constants k_{T1} and $\mu_{T,t}$ do not appear in equation 2.2 because thay do not vary from one run to another and, therefore, they play no role in the optimization. The logarithmic transformation expresses the quality loss in a decibel scale.

Similarly, total nominal-the-best quadratic quality loss due to thickness variance across-the-wafer and across-the-load is given by,

$$QL_{T2} = k_{T2}\,\mu_{T,t}^2\left(\frac{\sigma_T^2}{\mu_T^2}\right) \qquad (2.3)$$

where k_{T2} is the film thickness quality loss coefficient for a batch, μ_T is the mean thickness for the batch and σ_T is the overall standard deviation for the batch (see Appendix B). The signal-to-noise ratio SN_{T2} for equation 2.3 is given by,

$$SN_{T2} = -10\log_{10}\left(\frac{\sigma_T^2}{\mu_T^2}\right) \tag{2.4}$$

As before, constants k_{T2} and $\mu_{T,t}$ do not appear in equation 2.4 .

2) Growth Rate Cost: An enhancement in growth rate of the film leads to shorter deposition time for achieving target thickness. The cost function, as discussed in Appendix B, is given by,

$$C_G = k_G \mu_{T,t}\left[t_o \frac{1}{n_w}\sum_{i=1}^{n_w}\left(\frac{1}{\mu_{T,i}}\right)\right] \tag{2.5}$$

and the corresponding decibel scale signal-to-noise ratio SN_G is given by,

$$SN_G = -10\log_{10}\left[\frac{1}{n_w}\sum_{i=1}^{n_w}\left(\frac{1}{\mu_{T,i}}\right)\right] \tag{2.6}$$

where k_G is the growth rate cost coefficient, and t_o is the deposition time. The constant terms in equation 2.5 do not appear in equation 2.6 for the reason discussed before.

It is important to note that the cost function in equation 2.5 is not a cost due to quality loss because the load is never unacceptable even if the growth rate falls indefinitely. To counter the fall in growth rate the adjustment factor of deposition time is increased, thereby incurring increased fixed costs for labor, floor space, and equipment. The cost C_G consists of the labor cost C_L, the floor space cost C_F, the equipment cost C_E.

3) Resistivity Cost: The target was to minimize the resistivity of the film by controlling the process parameters. Resistivity is a continuous and non-negative quality characterstic with no adjustment factor in the deposition process. Therefore, we simply minimized the quadratic quality loss without adjustment [14], given by,

$$QL_\rho = k_\rho\left[\frac{1}{n_w}\sum_{i=1}^{n_w}\mu_{\rho,i}^2\right] \qquad (2.7)$$

where $\mu_{\rho,i}$ is the mean resistivity across the ith wafer in a batch, and k_ρ is the resistivity quality cost coefficient. Minimizing QL_ρ in equation 2.7 is equivalent to maximizing smaller-the-better signal-to-noise ratio SN_ρ given by,

$$SN_\rho = -10\log_{10}\left[\frac{1}{n_w}\sum_{i=1}^{n_w}\mu_{\rho,i}^2\right] \qquad (2.8)$$

As before, we ignored the constant k_ρ and expressed the quality loss in decibel scale.

4) Total Quality Cost: In order to find an optimal point for the process parameters with the constraint of the tradeoff between the three responses considered, i.e. the growth rate, film thickness uniformity, and the resistivity, a total quality loss function was considered. It was the equally weighted sum of the costs in equations 2.3, 2.5 and 2.7 and is given by,

$$QL_{overall} = QL_{T2} + C_G + QL_\rho \qquad (2.9)$$

This total quality cost is expressed in a decibel scale to give an overall signal-to-noise ratio,

$$SN_{overall} = -10\log_{10}\left[QL_{T2} + C_G + QL_\rho\right] \qquad (2.10)$$

The target was to minimize the total cost in equation 2.9 by maximizing the $SN_{overall}$ in equation 2.10 .

The cost coefficients, as determined in Appendix B, are given by,

$$k_{T2} = \frac{A_o}{\Delta_{T2}^2} \left[\frac{\$}{(A^\circ)^2}\right] \qquad (2.11(a))$$

$$k_G = (c_L + c_F + c_E)\left(1 + \frac{t_1}{t_o^*}\right) \left[\frac{\$}{min}\right] \qquad (2.11(b))$$

$$k_\rho = \frac{A_o}{\Delta_\rho^2} \left[\frac{\$}{(\Omega\_cm)^2}\right] \qquad (2.11(c))$$

where A_o is the $ cost incurred in discarding the entire batch when the batch non-uniformity exceeds Δ_{T2} angstroms (A°) for a target thickness of $\mu_{T,t}$ A°, or resistivity overshoots the functional limit of Δ_ρ Ω_cm on a target resistivity of μ_ρ Ω_cm (Note that ideally this target is zero). The terms c_L, c_F, c_E represent the fixed cost rate ($/min) for labor, floor, and equipment respectively. Also the total predeposition and postdeposition steps time t_1 is fixed for all runs. Time t_o^* represents the time it takes for the deposition step to achieve target thickness.

2.4.2 ANOVA Analysis

After doing the cost function analysis of the observed data, the next step was to estimate the main effects of the process parameters and to perform analysis of variance (ANOVA) [16]. Analysis of variance of the data gave the relative effect of the process parameters on the response considered. From this the most significant main effects were determined. ANOVA was performed for all the different cases of SN ratios discussed above.

3. *"Smart Response Surface"* PROCESS MODELLING

Data have no meaning in themselves; but they assume meaning in relation to a conceptual model of the phenomenon under scrutiny. In this chapter it is attempted to utilize the partial understanding of the in-situ doped polysilicon process and combine it with the empirical data to evolve a semi-empirical or a "Smart Response Surface" model based on dimensional analysis. The underlying motivation for the semi-empirical approach is to do without the intricacies of mechanistic modelling, such as the solving of three dimensional differential equations for mass transport and reaction kinetics, without sacrificing the causal accuracy of the predictions of the resultant model. This causal accuracy is achieved by combining the process variables into dimensionless groups which are physically more intuitive than the primitive process variables.

3.1 Process Background

Low pressure chemical vapor deposition (LPCVD) in hot walled reactors is rapidly replacing the conventional atmospheric pressure CVD (APCVD) method of depositing films on the wafers for various applications in microelectronics technology. The LPCVD method for producing thin insulators and semiconductor films gives reduced processing cost and superior product quality in terms of fewer defects, better thickness uniformity, and substantially improved step coverage than APCVD films. The close spaced, stand-up configuration for device wafers permissible in LPCVD reactors (Fig.3.1) leads to greatly increased throughput[1] despite the reduced film deposition rates.

[1] load size divided by deposition cycle time

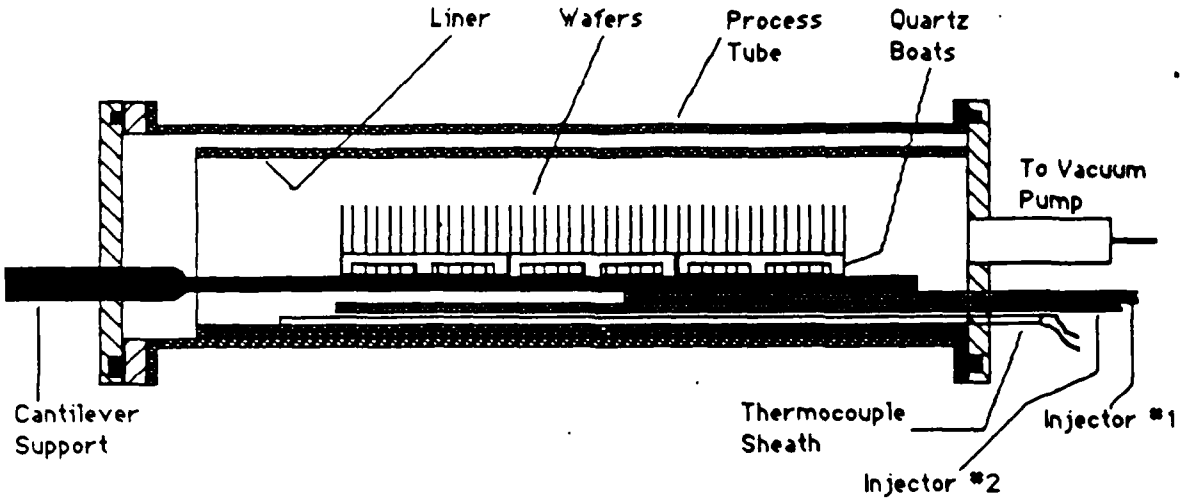

Fig. 3.1: Schematic of a LPCVD Reactor

The LPCVD technique for depositing polycrystalline silicon films by the pyrolysis of silane (SiH_4) yields very uniform films because at reduced pressure diffusion is rapid enough so that the chemical reactions at the wafer surface, and not the gas phase mass-transfer process, are the rate controlling factors[2, 11]. However, the application of LPCVD to the *in-situ* phosphorus doped polycrystalline process degrades the polysilicon LPCVD process because of the phosphine gas (PH_3) introduced into the furnace along with silane, [4, 5]. This logical extension of the intrinsic polysilicon process is desirable because it avoids the complexity of more conventional doping techniques such as post-deposition implantation of dopant, or indiffusion of dopant from a dopant rich layer applied on the silicon surface, and offers lower film resistivity because of more uniform incorporation of phosphorus. But the introduction of phosphine into the system severly suppresses the growth rate, leads to within-wafer and wafer-to-wafer film thickness non-uniformities, and poses a problematic tradeoff between growth rate, thickness uniformity, and resistivity [8, 9].

The most widely accepted explanation for the problems of growth rate suppression and film inhomogeneties is that phosphine passivates the silicon surface by altering the silicon growth kinetics

[4, 5]. A lone pair of electrons on the phosphine molecule helps it to compete successfully with silane (a fully coordinated molecule) for the active surface sites and form a layer of nondissociative pentavalent phosphorus bridging with adjoining silicon atoms. This exclusion of silane from the heterogeneous chemistry leads to tremendously lower growth rates. It has been shown that the adsorption of phosphine proceeds about 40 times faster than that of silane [4].

The second problem of film non-uniformities renders the films unfit for use in the VLSI applications. The films deposited in this process have highest growth rate along the edge of the wafer and reduce to a minimum at the wafer center (Fig3.2). This growth rate gradient is directly related to the concentration gradient of the active species in the interwafer region. Also, the active species participating in the film deposition is no longer silane (it is suppressed by phosphine) but silylene (SiH_2), a homogeneous species resulting from the pyrolysis of silane

$$SiH_4(g) \quad <-----> \quad SiH_2(g) + H_2(g)$$

Silylene has an activation energy comparable to that of phosphine (both have a lone pair of electrons) and, therefore, can successfully insert into the Si-H bonds on the silicon surface. The suppression of the heterogeneous chemistry of silane (a majority homogeneous species) by phosphine and the fractional contribution of silylene (a minority homogeneous species) to the growth rate indicates that this process, in contrast with the intrinsic polysilicon LPCVD, is mass transport limited and not surface kinetic controlled [11]. Thus, the depletion of the active silylene species in the interwafer region results in the growth rate profiles shown in Fig3.2. This depletion effect, or *bull's eye effect* - as it is called, can also be looked upon as the silylene contribution from the annular region depositing on the wafer edges. To exclude the annular silylene from interwafer region and, therefore, improve the growth rate uniformity, it is

recommended that the wafer load be placed in a cage with a surface area large enough to consume the annular silylene.

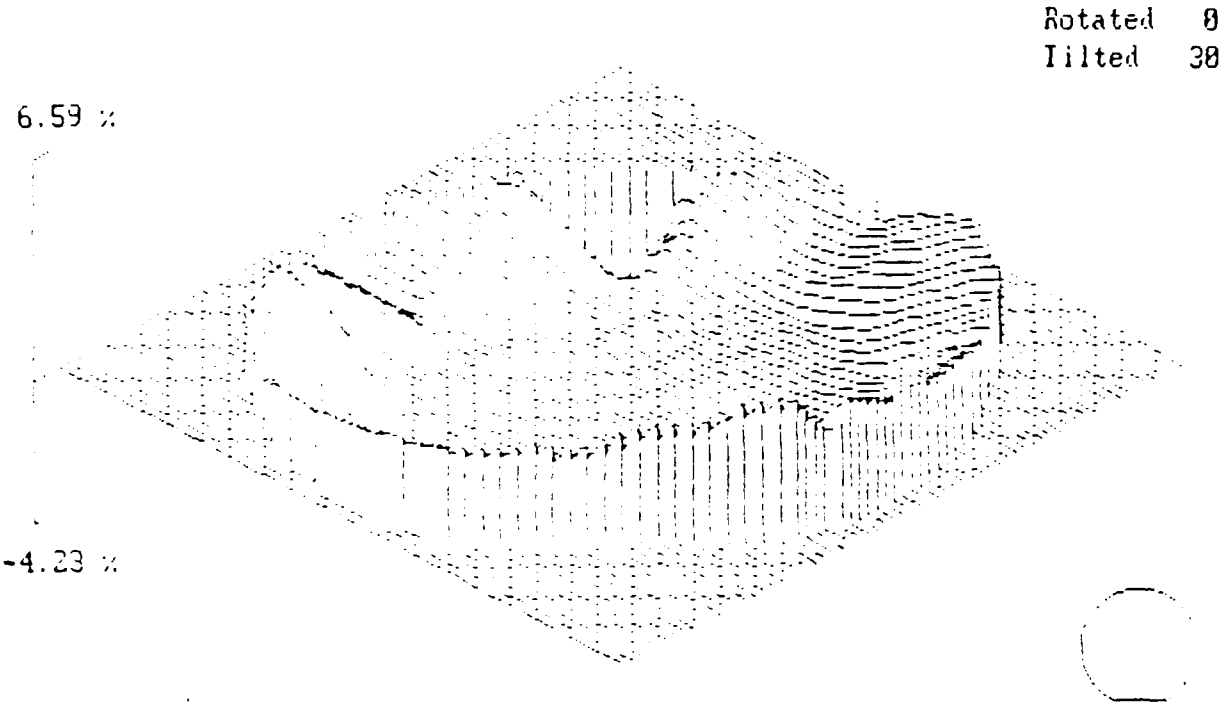

Fig. 3.2: Typical Growth Rate Profile in In-Situ Doped Polysilicon Process

3.2 Dimensional Analysis Model Formulation

A model is developed for the tradeoff between the growth rate mean μ and nonuniformity (measured by standard deviation σ) by considering the following "signal-to-noise" (SN) ratio as the desired response for each individual wafer in a batch

$$SN = -10\log_{10}\left(\frac{\sigma^2}{\mu^2}\right) \qquad (3.1)$$

The stated goal is to optimize the process under consideration i.e. increase SN ratio by means of a parallel design of experiments (DOE)[1] and compare the DOE predictions with that of the SN model. In the process of doing so, the strength of dimensional analysis as a Smart Response Surface methodology will be demonstrated.

Consider the "reaction cell" shown in Fig.3.3. Of all the geometrical parameters shown, only interwafer distance "w" and the cage hole radius "r_h" are the geometrical variables. From here on all other constant length parameters are referred to as "L_i" .

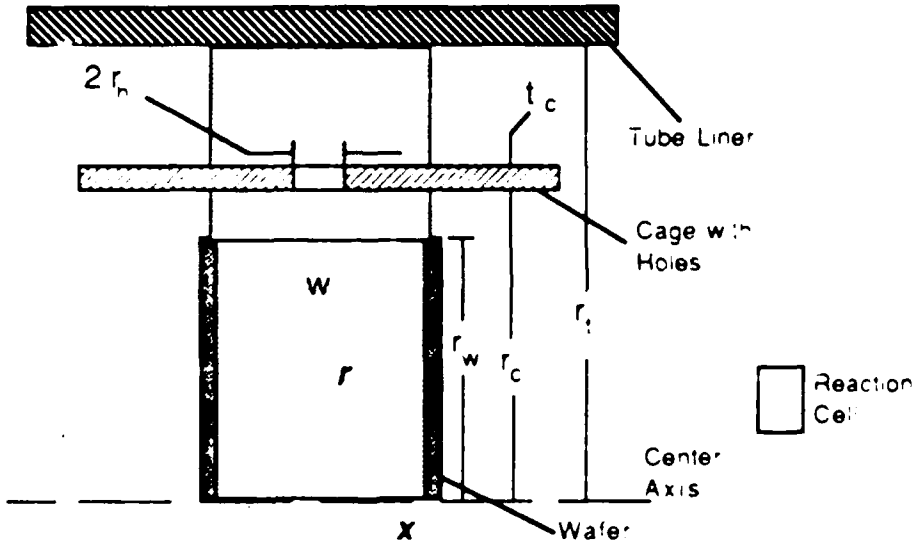

Fig.3.3: Schematic of the "Reaction Cell"

The following process parameters (with their dimensions) are identified and considered:

(Process Variables)

- Interwafer distance (**w**) [**L**],
- Hole radius on the cage ($\mathbf{r_h}$) [**L**],
- Deposition temperature ($\mathbf{T_d}$) [**θ**],
- Deposition pressure (**P**) [$\mathbf{M/LT^2}$],

[1] See Chapter 2 for a discussion on SN ratios.

- Inter-injector distance (I_x) [L].
- Total silane flow (Q_s) [M/T].
- Phosphine flow through injector #1 (Q_{p1}) [M/T].
- Phosphine flow through injector #2 (Q_{p2}) [M/T].
- Multicomponent Gas Diffusivity (D_{ij}) [L^2/T].

(Process Constants)

- Constant geometrical parameters (L_i) [L].
- Ideal Gas Constant (R_o) [$ML^2/T^2\theta$].
- Activation Energies (E_i) [ML^2/T^2].
- Molecular weights of various species (M_i) [M].
- Film surface densities of various species (ρ_i) [M/L^3].

(Process Response)

- Response Parameter (SN) [-0-].

The diffusivity D_{ij} is defined by T_d, P, M_i, and R_o and, therefore, can be neglected. Similarly, ρ_i is neglected because it is defined by M_i and L_i. At this stage we have 12 process parameters (8 variables plus 4 constants).

Having listed the significant process parameters, the **Pi Theorem of Dimensional Analysis** is utilized to develop a set of dimensionless variables called the *Pi Groups*. These Pi groups must satisfy the condition of *dimensional homogeneity* i.e. all the Pi groups in an additive model must have the same dimensions. Since the response SN is dimensionless, all other Pi groups must also be dimensionless for any meaningful solution to the process. From the above parameter list, one parameter (variable or constant) for each dimension (length **L**, time **T**, mass **M**, and temperature θ) is selected, making sure that the parameters chosen, called the *primary parameters* from hereon, are dimensionally independent i.e. they cannot be "power grouped" into a dimensionless Pi group. The primary parameters selected are:

- Constant geometrical parameter (L_i) for length dimension,

- Molecular weight (M_i) for mass dimension,
- (R_0)/(E_i) for temperature dimension,
- Pressure (**P**) for time dimension.

It can be shown that there is no power grouping of these primary parameters which is dimensionless. Even though we can cancel mass, length, and time dimension, no power group involving these primary parameters rids itself of the temperature dimension. Also, having selected 5 of the above mentioned 12 process parameters as the primary parameters, Pi theorem states that the number of Pi groups should be no more than 7.

Now comes the most critical step of using these primary parameters to nondimensionalize other parameters, called *secondary parameters* from hereon. This is where the secondary parameters are grouped with primary parameters on the basis of some understanding about the physical reality of the process under consideration. Only secondary process variables need to be nondimensionalized because the process constants merge with a common constant term C_0 in an additive model for the process response.

Geometrical variables are nondimensionalized by L_i to give the following Pi groups,

$$\Pi_1 = \frac{w}{L_i} \tag{3.2}$$

$$\Pi_2 = \frac{r_h}{L_i} \tag{3.3}$$

$$\Pi_3 = \frac{I_x}{L_i} \tag{3.4}$$

Deposition temperature will interact with the activation energies to determine the rate of silylene production in the gas phase and also the adsorption of various species onto the polysilicon film. This gives us a Pi group,

$$\Pi_4 = \frac{E_1}{R_o T_d} \tag{3.5}$$

The variation in depostion temperature is expected to influence the concentrations in gas phase, given by $(P/R_o T_d)$, but this influence is found to be very small because of a very limited range of pressure and temperature levels allowed for this process. The flow rates are nondimensionalized by pressure to give the following Pi groups,

$$\Pi_5 = \frac{Q_s}{\sqrt{PM_1L_1}} \tag{3.6}$$

$$\Pi_6 = \frac{Q_{p1}}{\sqrt{PM_1L_1}} \tag{3.7}$$

$$\Pi_7 = \frac{Q_{p2}}{\sqrt{PM_1L_1}} \tag{3.8}$$

For the process under consideration, the fraction of phosphine to silane, and not the phosphine flow, is the controlling parameter. Therefore, equation 3.6 is divided by equations 3.7 and 3.8 to obtain physically more significant Pi groups,

$$\Pi_6^* = \frac{Q_s}{Q_{p1}} \tag{3.9}$$

$$\Pi_7^* = \frac{Q_s}{Q_{p2}} \tag{3.10}$$

Based on these Pi groups the functional relation can be expressed as

$$SN = \mathbf{f}\left(\Pi_1, \Pi_2, \Pi_3, \Pi_4, \Pi_5, \Pi_6^*, \Pi_7^*\right) \tag{3.11}$$

This functional relation indicates two advantages of dimensional analysis. Firstly, the number of process parameters is reduced from 12 (or 8 process variables) to seven Pi groups. Therefore, for the future usage of the model described below we need to do fewer

numbers of experiments because the number of variables have reduced. Secondly, the Pi groups above are physically more significant. This infusion of physical knowledge is enunciated further below.

An appropriate functional relation was reached by starting with a first order polynomial of all Pi groups. All these first order main effects were retained in the subsequent steps. To this model various second order terms were added and/or deleted by using *stepwise regression* with T-tests[1] as the deciding criterion. Then the partial understanding of the physics of the process was used to include some physically sensible interactions. Finally, for the purposes of regression evaluation of an additive model for SN ratio, the following 13 term equation was used.

$$SN = C_0 + C_1(w) + C_2(r_h) + C_3(T_d) + C_4(I_x) + C_5\left(\frac{Q_s}{\sqrt{V}P}\right) + C_6\left(\frac{Q_s}{Q_{p1}}\right) + C_7\left(\frac{Q_s}{Q_{p2}}\right) + C_8\left(\frac{Q_s}{Q_{p1}}\right)^2 + C_9(I_x^2) + C_{10}(T_d)\left(\frac{Q_s}{Q_{p1}}\right) + C_{11}(I_x)\left(\frac{Q_s}{Q_{p1}}\right) + C_{12}(I_x)\left(\frac{Q_s}{Q_{p2}}\right) \qquad (3.12)$$

Note that the constant parameters shown in equation 3.2 to 3.11 merge with the calibration coefficients C_o, C_1, ..., and C_{12} in equation 3.12. Descriptive use of this regression model emphasized precise estimation of regression coefficients by using the data from L18 orthogonal array experiments, and predictive use focused on the minimization of the prediction errors.

---

[1] The T-test says that a regression coefficient C_i is significant i.e. not zero if : $|t| > t(1-k/2; d)$ where,
t = (Calculated Value of C_i)/(mean square error in that Value of C_i);
k is the confidence level; and
d is the number of degrees of freedom for C_i

Various interactions included in equation 3.12 require some discussion. Deposition temperature interacts strongly with the major phosphine fraction flowing through injector #1 because it controls the relative adsorption and desorption of phosphine onto the wafer surface. The interaction of temperature with phosphine fraction through injector #2 is found to be not very significant.

The interaction of R_h with (Q_s/Q_{p1}) and (Q_s/Q_{p2}) was expected to be significant because it determines the amount of flow through the cage. However, this interaction was neglected because stepwise regression results indicated otherwise.

As one moves away from the load end of the tube the axial depletion effects become significant. Therefore, I_x interacts strongly with (Q_s/Q_{p1}). However, near the load end there are no significant axial depletion effects and, therefore, the interaction of I_x with (Q_s/Q_{p1}) through injector #1 (fixed in position) is not expected to be significant. The presence of this interaction in the above model for the load end wafers may distort the corresponding predictions to a certain extent. The phosphine fraction flowing through injector #2 plays an important role with regard to the position of the adjustable injector #2 because the position of injector #2 determines if the phosphine flowing through it will remain trapped in a homogeneous phase complex called monosilylephosphine (SiH_3PH_2), hence, the interaction of I_x with (Q_s/Q_{p2}). This complex is formed by the gas phase reaction of silylene and phosphine [4, 5] and is unstable above 550°C in the presence of surfaces. Therefore, if injector #2 injects the gases at a point, say, beyond the heated load zone, i.e the region between load end of the tube and wafer #1, then this complex will tend to trap more of phosphine from injector #2 because there is lesser surface area and lower temperature in this region. Entrapment of more phosphine should lead to better uniformities across the wafer and higher growth rates (especially near the load end) in this transport limited process (see the behavior of SN_{T1} and SN_G in Chapter 5). This and other observations mentioned above

were confirmed by the behavior of equation 3.12 to the experimental data (see Chapter 5).

The dimensional analysis model was compared to the corresponding primitive variables model which was evolved by using the step regression method discussed before. All the first order main effects and the interactions corresponding to the ones in equation 3.12 were considered in this primitive variables model. Therefore, a 13 terms model for a design involving 8 primitive parameters was determined as.

$$SN = C_0 + C_1(w) + C_2(r_h) + C_3(T_d) + C_4(P) + C_5(I_x) + C_6(Q_s) + C_7(Q_{p1}) + C_8(Q_{p2}) + C_9(I_x^2) + C_{10}(T_d)(Q_s) + C_{11}(I_x)(Q_s) + C_{12}(I_x)(Q_{p1}+Q_{p2}) \quad (3.13)$$

Note that the interwafer distance "w" is regressed only to a linear term because it has only two levels in the L18 orthogonal array.

4. EXECUTION OF EXPERIMENTS

Based on the experimental design discussed in the chapter 2, the experiments were performed in the process lab at BTU Engineering. Before exposing the wafers to the *in-situ* Phosphorus Doped Polysilicon Process, each wafer was treated with a wet oxidation process to grow a 1000 A^{o} oxide film on <100> type silicon substrate.

4.1 Equipment Description and Procedure

The film deposition was done in a commercial BTU Engineering/Bruce Systems 7351C horizontal, hot-wall diffusion furnace with three zone temperature profile control maintaining the desired temperature in a 32 inch long load zone(see Fig. 2.1). The furnace tube was lined with a quartz liner. The total production load of 114 wafers, placed in a 32 inch flat temperature profile load zone on a paddle, consisted of three quartz boats with 38, 4 inch, 575 micron thick wafers each. Of these 114 wafers, 12 were test wafers and then rest were dummy wafers.

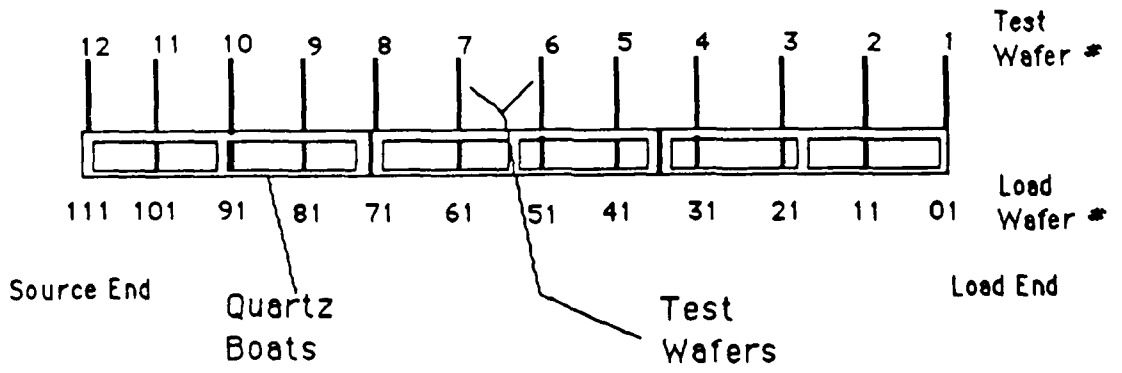

Fig.4.1: Test Wafers Position in the Load

The position of the test wafers is shown in Fig.4.1. The interwafer distance "w", as discussed in the last chapter, had two levels - every

slot in the boat (7.5 mm apart) or every other slot in the boat (15 mm apart). The deposition pressure was held at a constant value by regulating the pump cross-section with a butterfly valve controlled from a feedback control circuit. The inter-injector distance "I_x" was changed after each run by moving the adjustable injector #2. Three sets of quartz cages with different hole areas were used and their ends were covered shut with quartz baffles. Two silane mass flow controllers with 300 sccm capacity each and two phosphine mass flow controllers with a capacity of 10 sccm (for injector #1) and 6.2 sccm (for injector #2) were used.

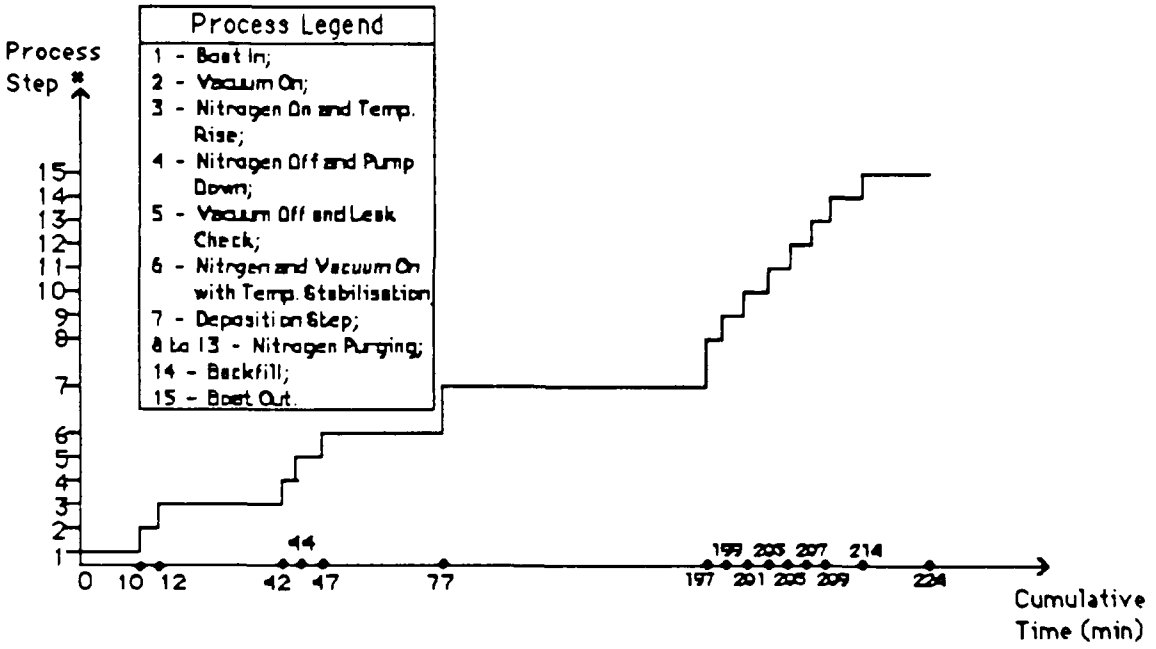

Fig.4.2: In-situ Phosphorus Doped LPCVD Process Recipe

The 7351 microprocessor recipe used to run the furnace is shown in Fig.4.2. The process parameters of step #7 in the recipe above were varied from one run to another but the same recipe was followed with a deposition run of two hours. The eighteen experiments outlined in the L18 orthogonal array in Fig.2.2 were performed in a random order so that the statistical bias was minimized.

The processed wafers were then annealed at 1000°C for 30 minutes in a slightly oxidizing atmosphere of 95 vol % N_2 and 5 vol % O_2 in order to prevent the outdiffusion of the dopant phosphorus. The thin SiO_2 film formed during annealing was removed by 7:1 buffer oxide etch before data acquisition.

Test wafers #2, #7, and #11 were then measured for film thickness with a Prometrix SM2000 SpectraMap system. Film thickness mean and variance for a wafer was obtained from 49 readings at points shown in Fig.4.3 The required refractive index adjustment factor (which varies with the dopant concentration and the deposition temperature) was obtained for each run from correlation with the Dektak surface profilometer thickness readings. This adjustment factor was consistently found to almost 1.0. Therefore, the influence of the variation of refractive index on thickness readings from the Prometrix was concluded to be small and, hence, neglected for the purpose of the decibel scale SN ratios. The film resistivity was obtained from the Prometrix automatic four point probe readings for sheet resistance.

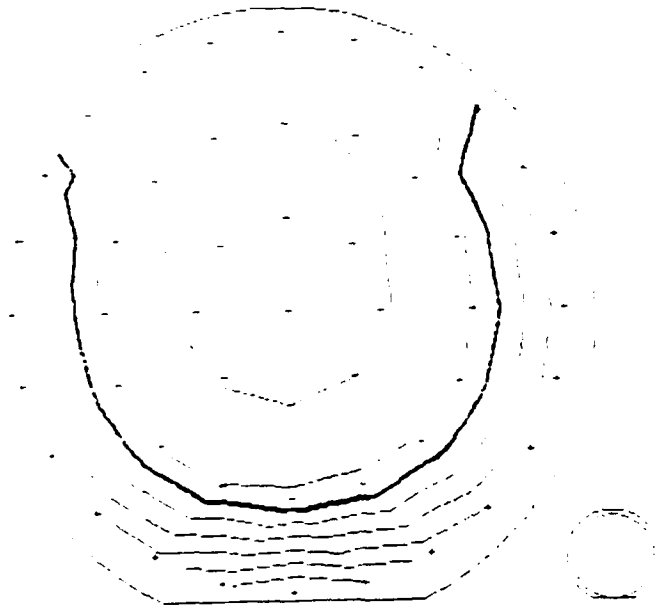

Fig.4.3: Typical Thickness Profiles with the Points of Measurement by Prometrix SM2000 Spectramap System on a 4 inch Wafer

5. RESULTS AND DISCUSSION

The observed data is tabulated in Appendix A in Tables A.1(1) to A.1(18). The measured data was subjected to the analysis outlined in chapter 2. The process parameters in the L18 design were optimized according to signal-to-noise (SN) ratios outlined in equation 2.2, 2.4, 2.6 and 2.8:

$$SN_{T1} = -10 \log_{10}\left[\frac{1}{n_w} \sum_{i=1}^{n_w} \left(\frac{\sigma_{T,i}^2}{\mu_{T,i}^2}\right)\right] \qquad (2.2)$$

$$SN_{T2} = -10 \log_{10}\left(\frac{\sigma_T^2}{\mu_T^2}\right) \qquad (2.4)$$

$$SN_G = -10 \log_{10}\left[\frac{1}{n_w} \sum_{i=1}^{n_w} \left(\frac{1}{\mu_{T,i}}\right)\right] \qquad (2.6)$$

$$SN_p = -10 \log_{10}\left[\frac{1}{n_w} \sum_{i=1}^{n_w} \mu_{p,i}^2\right] \qquad (2.8)$$

The values for these SN ratios are shown in Table 5.1 and the corresponding averaged main effects for the process parameters are shown in Table 5.2. These main effects for a particular factor level setting were determined by averaging the SN ratio for the experiments in which that particular factor level was used. For example, the SN ratios for experiments 1 to 9 were averaged to obtain the main effect (in decibels) of "w" at level 1 on the corresponding response. The results in Table 5.1 and 5.2 were used to decide upon the optimum levels of the process parameters based on the criterion of maximizing the corresponding SN ratio.

SN ratios / Run #	SN_{T1}	SN_{T2}	SN_G	SN_p
1.	46.992	18.118	35.990	-22.126
2.	31.712	26.545	34.156	-18.190
3.	25.493	18.124	34.090	-18.848
4.	24.647	20.569	30.132	-19.388
5.	40.843	20.215	38.662	-31.477
6.	26.250	23.123	35.407	-20.385
7.	25.455	11.285	33.412	-17.251
8.	21.246	17.299	33.747	-17.717
9.	31.383	15.597	37.912	-24.884
10.	37.344	22.045	36.040	-18.996
11.	27.794	22.159	34.459	-17.358
12.	29.745	11.358	36.112	-19.363
13.	24.804	21.563	33.202	-17.339
14.	25.936	10.210	36.631	-17.110
15.	27.719	23.683	38.060	-21.258
16.	31.473	24.642	37.025	-18.530
17.	22.373	12.458	35.485	-16.931
18.	21.762	18.990	36.921	-17.062

Table 5.1: SN ratios for Orthogonal Array Runs

5.1 Film Thickness Profile and Growth Rate Analysis

The main effects of the process parameters on the overall batch variance (i.e. SN_{T2}) and across-the-wafer variance (i.e. SN_{T1}), and growth rate (i.e. SN_G) are plotted in the marginal plots in Fig.5.3 and 5.4. The optimum factor level settings, corresponding to the highest SN's, are shown in Fig.5.3 and 5.4. Tables A.2, A.3,

SN Ratios		SN_{T1}	SN_{T2}	SN_G	SN_P
Factor	Levels				
W	1	30.447	18.986	34.834	-21.137
	2	27.661	18.567	35.993	-18.218
A_c	1	33.180	19.725	35.141	-19.147
	2	28.366	19.894	35.349	-21.160
	3	25.616	16.714	35.750	-18.726
T_d	1	31.786	19.706	34.300	-18.939
	2	28.318	18.148	35.524	-19.794
	3	27.059	18.479	36.417	-20.300
P	1	30.151	18.764	35.340	-20.327
	2	29.054	18.328	35.411	-20.114
	3	27.957	19.241	35.490	-18.592
I_x	1	29.134	17.317	35.470	-18.549
	2	27.257	20.683	34.872	-19.068
	3	30.374	18.334	35.898	-21.415
Q_s	1	28.568	17.320	34.991	-18.973
	2	28.797	18.993	35.299	-19.272
	3	29.797	20.020	35.951	-20.787
Q_{P1}	1	34.395	16.690	37.056	-22.248
	2	28.476	19.859	35.427	-18.838
	3	24.291	19.784	33.759	-17.946
Q_{P2}	1	32.651	20.058	36.570	-21.433
	2	28.903	22.272	35.360	-19.448
	3	25.608	14.003	34.310	-18.151

Table 5.2: Main Effects of the Process Parameters

and A.4 in Appendix A show the ANOVA results for SN_{T1}, SN_{T2}, and SN_G respectively. ANOVA results indicate that phosphine flow rates are the most significant parameters influencing the film thickness profile and the growth rate. Batch variance is also strongly influenced by cage hole area, inter-injector distance, and silane flow rate. Variance across the wafer depends on cage hole area, deposition temperature, and interwafer distance as well. Growth

rate is influenced significantly by deposition temperature, and interwafer distance as well.

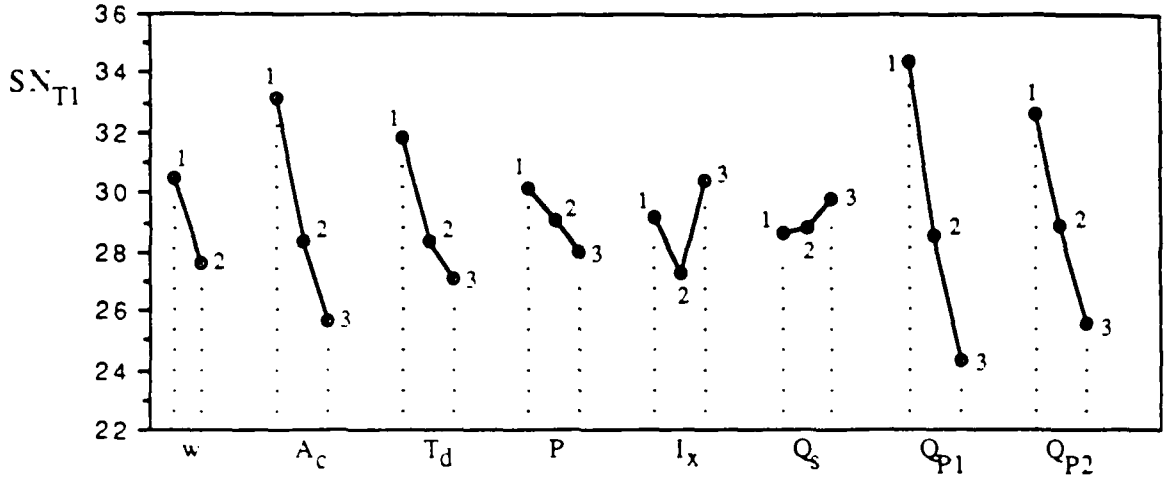

Fig. 5.3: Marginal Plots for SN_{T1}

It was observed that the film thickness uniformity degrades (i.e. SN_{T1} in Fig. 5.3 and SN_{T2} in Fig. 5.4 *falls) with rising interwafer* distance "w". This is explained by the fact that wider "w" means that more silylene (SiH_2) per wafer is coming into the interwafer region from the tube-cage annulus. This "excess" SiH_2 deposits near the wafer edges to cause higher nonuniformity. This also leads to slightly increased average growth rate and, therefore, the SN_G rises with increasing "w" in Fig.5.5.

Increased % hole area "A_c" in the cage worsens across-the-wafer uniformity (Fig.5.3) because of the rise in the amount of SiH_2 flowing in from the annulus. Batch variance (Fig. 5.4) is not influenced strongly by "A_c" for lower levels but at 20% hole area the consumption of the annular SiH_2 is so rapid that the increased depletion effects lead to a rise in batch variance. Therefore, SN_{T2} falls rapidly. Again, the increased consumption of the annular SiH_2 leads to slightly increased average growth rates (Fig.5.5).

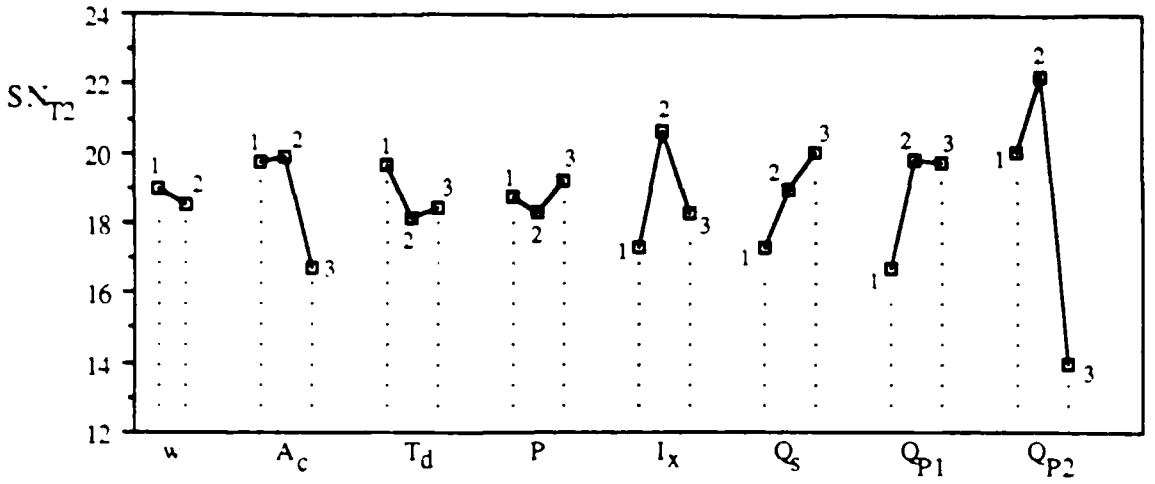

Fig. 5.4: Marginal Plots for SN_{T2}

The film thickness uniformity degrades and the average growth rate rises with increasing deposition temperature "T_d". Increasing growth rate with temperature is explained by the rising rate of production of SiH_2 (the dominant surface reactant) in the homogeneous phase (Fig.5.5). However, film nonuniformity rises for temperature upto 600°C and then changes very little (Fig.5.3 and Fig. 5.4). Probable cause for this behavior is the relative contribution of various gas phase species involved in the polysilicon film deposition. Upto 600°C the increased contribution of SiH_2 from the larger volume of the annular region accounts for the nonuniformity. For higher temperatures other highly reactive gas phase minority species like disilane (Si_2H_6), that add to the nonuniformity, become extremely unstable and, therefore, their contribution to the heterogeneous chemistry (i.e surface reactions) is reduced. Also, at nigher temperature silane (SiH_4), the majority species in the gas phase, becomes more active in attacking the surface sites successfully and this makes the growth rate kinetics tend towards kinetic control and higher uniformity rather than transport limited control. Therefore, there is no further rise in the nonuniformity. The existence of these various parallel reaction mechanisms has been well documented [4, 5] but the experimental verification of the above reasoning is required.

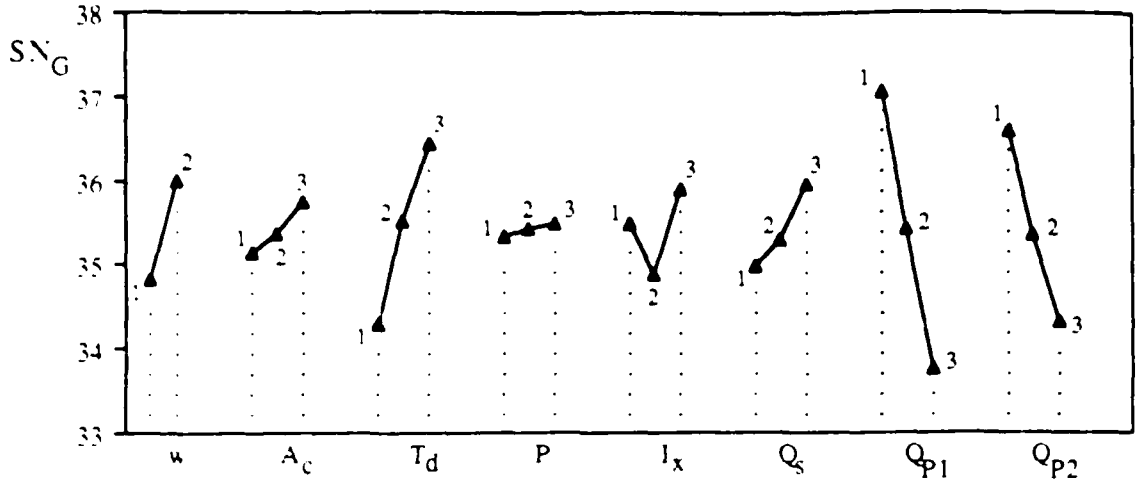

Fig. 5.5: Marginal Plots for SN_G

The influence of rising pressure on batch variance (Fig. 5.4) is not very significant but the film nonuniformity across the wafer rises appreciably with rising pressure (Fig.5.3). Rising pressure means a higher SiH_2 concentration and, therefore, a higher growth rate (Fig.5.5). Although rising pressure means a higher phosphine (PH_3) concentration as well, it can be shown by order of magnitude analysis that the change in the PH_3 concentration with pressure is lower than that of SiH_2. In any case, the rise in PH_3 concentration does have a dampening effect on the rise in growth rate and, therefore, the rise shown in Fig.5.5 is not very significant.

The overall batch variance improves for the middle level of inter-injector distance "I_x" (Fig. 5.4) but the across-the-wafer variance and growth rate are worst for this level (Fig.5.3 and 5.5). The influence of "I_x" on the film thickness properties is not well understood except for a possible linkage between gas phase SiH_3PH_2 complex and the point where the gases from injector #2 are released into the tube with respect to the position of the heated load zone. This is briefly discussed in section 3.2 of chapter 3.

Thickness variance invariably falls (Fig5.3 and Fig. 5.4) and growth rate rises (Fig.5.5) with rising silane flow rates. Uniformity across the wafer improves with rising silane flow rates possibly because part of annular SiH_2 is blown away at higher silane flows.

As expected, the thickness variance across the wafer rises with an increase in the phosphine flow rates (Fig.5.3 and Fig. 5.4). This is because of the change in the reaction mechanism from being kinetic limited to transport limited with rising dopant gas concentration. Increased PH_3 means more poisoning of the substrate and, therefore, a substantially lower growth rate(Fig.5.5). The influence of PH_3 on batch variance is different for "Q_{p1}" and "Q_{p2}" probably because of the effect of "I_x".

5.2 Resistivity Data Analysis:

Marginal plots in Fig.5.6 show the main effects of the process parameters on the average resistivity of the in-situ phosphorus doped polysilicon film. The corresponding ANOVA analysis for smaller-the-better resistivity SN ratio (SN_ρ) is given in Table A.5 in Appendix A. Phosphine flow rates, interwafer distance, inter-

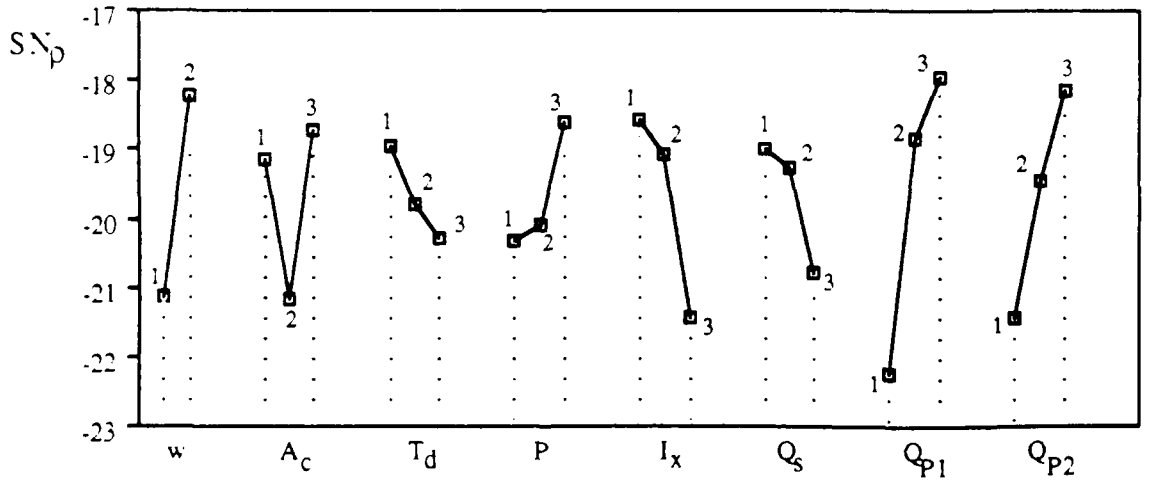

Fig. 5.6: Marginal Plots for SN_ρ

injector distance, and cage hole area have major effect on resistivity. Note that the effort here was to reduce the average resistivity across the wafer in a load.

Increased "w" means a higher growth rate of the film and, therefore, larger grain size. Also, resistivity is seen to fall with rising thickness [9]. Therefore, S_{N_ρ} rises with increase in "w".

Increasing film growth rate with rising "A_c" leads to a higher resistivity (i.e. lower S_{N_ρ}) but the effect reverses for very high "A_c". It is also observed that the variance of resistivity across a wafer increases dramatically for high levels of "A_c". This indicates that there is an increased contribution of PH_3 from the annular region to the interwafer region at very high hole area. Therefore, for large holes, the probable cause for lower resistivity is that the increased influx of annular PH_3 content overshadows the rise in thickness due to increasing influx of annular SiH_2 and this raises the dopant density in the film.

Deposition temperature rise leads to higher resistivity because of the enhanced desorption of phosphorus from the silicon surface. At higher deposition temperature the grain size of polysilicon is small and this too leads to higher resistivity.

Rising gas pressure means an increased partial pressure of PH_3. This means a rise in the phosphorus content of the film and, therefore, a fall in resistivity.

There is dramatic rise in resistivity with increase in the inter-injector distance. This behavior can again be explained by the role of gas phase SiH_3PH_2 complex. As discussed in Chapter 3, at highest level of I_x more of phosphine from injector #2 is trapped in a complex. Therefore, lesser amount of phosphine is available for the wafers. This leads to lower dopant density in the film and, hence, higher resistivity.

It has already been shown that a rise in silane flow leads to thicker film. Also, increased silane flow rate blows away part of the annular PH_3 (this is indicated by reduced variance in resistivity that is observed across the wafer with rising silane flow). These two facts explain the observation that there is a rise in average resistivity with increased silane flow.

Increased PH_3 flows increase the concentration of phosphine in the system. This leads to greater amount of phosphorus incorporation into the polysilicon film and, therefore, lower resistivity.

5.3 Verification Experiments:

In order to study the effectiveness of the orthogonal design of experiments, a set of confirmation runs were made based on the optimum levels for the process parameters predicted by the marginal plots. These optimum levels correspond to the highest SN ratio in the relevant marginal plots in Fig.5.3, 5.4, 5.5 & 5.6. The data for these runs is given in Table A.6 in Appendix A. Two modifications were made to the normal procedure of determining the optimum level of a process parameter as the one with highest SN ratio. Firstly, in order to avoid cutting the load size, only lower level of interwafer distance was used for the confirmation runs. Secondly, instead of using the optimum levels from the marginal graphs, second order, 16 terms linear regression equations for various SN ratios were evolved by using the 18 data points for each of the SN ratios. For instance, one of the regression equations was[1]:

---

[1] The units various parameters in equation 5.1 are:
$[w] = [\text{-}0\text{-}]$ i.e. just level #; $[A_c] = [\%]$; $[T_d] = [^oC]$; $[P] = [\text{mtorr}]$; $[I_x] = [\text{inches}]$; $[Q_s] = [\text{sccm}]$; $[Q_{p1}] = [Q_{p2}] = [\text{sccm}]$

$$SN_\rho = 2.367E+02 + (2.919E+00)(w) - (8.387E-01)(A_c) + (4.197E-02)(A_c^2) - (5.570E-01)(T_d) + (4.360E-04)(T_d^2) - (6.982E-01)(P) + (1.047E-03)(P^2) + (1.175E+00)(I_x) - (3.654E-02)(I_x^2) + (1.279E-01)(Q_s) - (2.430E-04)(Q_s^2) + (4.268E+00)(Q_{p1}) - (5.556E-01)(Q_{p1}^2) + (5.447E+00)(Q_{p2}) - (1.453E+00)(Q_{p2}^2) \quad (5.1)$$

From such equations the extrema regression predictions for the maxima of the relevant SN ratio were determined as the optimum.

SN Type	Process Parameters for confirmation Runs	SN ratio Values		Response Back-Calculated from Corresponding SN		
		predicted	observed	Response Type	Value	
					Best in L18	Confirmation Run
SN_{T1}	$w = .75$; $r_h = .125$; $T_d = 853.$; $P = 325.$; $I_x = 65.$; $Q_S = 350.2$; $Q_{p1} = .58$; $Q_{p2} = .26$	49.4	46.2	Across the Wafer Average Nonuniformity	0.45% (run #1)	0.49%
SN_{T2}	$w = .75$; $r_h = .328$; $T_d = 853.$; $P = 375.$; $I_x = 53.5$; $Q_S = 405.9$; $Q_{p1} = 2.87$; $Q_{p2} = .79$	31.1	32.2	Average Nonuniformity for a Batch (across wafer + down the load)	4.7 % (run #2)	2.5 %
SN_G	$w = .75$; $r_h = .783$; $T_d = 893.$; $P = 375.$; $I_x = 65.$; $Q_S = 350.2$; $Q_{p1} = .58$; $Q_{p2} = .26$	42.2	40.7	Average Growth Rate for a Batch	61.2 A°/min (run #5)	98.0 A°/min
SN_ρ	$w = .75$; $r_h = .125$; $T_d = 853.$; $P = 375.$; $I_x = 42.2$; $Q_S = 264.2$; $Q_{p1} = 3.07$; $Q_{p2} = 1.52$	−22.3	−21.9	Average Resistivity for a Batch	7.04e-4 ohm-cm (run #17)	12.45e-4 ohm-cm

Note: Units for Process Parameters are: $[w]=[r_h]=[I_x]=$[cm.]; $[T_d]=$[°K]; $[P]=$[mtorr]; $[Q_S]=[Q_{p1}]=[Q_{p2}]=$[sccm]

Table 5.3: Results of Confirmation Runs vs L18 Orthogonal Array Experimentation

For example, in equation 5.1 the derivative of SN_ϕ with respect to "I_x" is equated equal to zero to get a predicted optimum of I_x = 16.6 inches. In case of process parameters with negative slopes the extrema regression prediction is for the minima of the concerned SN ratio. Therefore, the marginal graph predictions for the optimum (i.e. maximum SN) were used for parameters with negative slopes. For example, the extrema for "A_c" corresponds to a minima in equation 5.1. The process parameter settings and the predicted SN ratios for the confirmation experiments are shown in Table 5.3.

As indicated before, a lack of data for determining the cost coefficients in equation 2.11 prevented us from performing a confirmation experiment for the overall optimum for the tradeoff responses of film thickness uniformity, growth rate, and resistivity.

Results of these confirmation experiments are tabulated in Table 5.3 which shows the observed and predicted SN ratios for these runs. The predicted SN ratios seem to be right on target except for SN_{T1}. This indicates that the additive model underlying the Taguchi method of process optimization is not sufficient for film thickness uniformity across the wafer. There are some important interactions that need to be considered for determining the optimal set of process conditions. Development of a semi-empirical model serves to this end.

The confirmation run result for SN_ϕ is not as good as the best run in L18 orthogonal array (run #17) because for the actual optimal run it was required that highest levels of interwafer distance and cage hole area be used for which the predicted optimal SN_ϕ was -8.9 i.e. a resistivity of .28 mohm-cm. But we used lowest level of "w" for the reason stated above. Also, a cage hole area of 0.5% was used so that the average resistivity is not only reasonably low (which 1.245 mohm-cm is) but also uniform across the wafer. It is important to point out that the average nonuniformity for sheet resistance in run #17 was 11% wheras for the SN_ϕ confirmation run it was only 4%.

Regression Coefficients	*Primitive Variables Model*			*Dimensional Analysis Model*		
	Estimated Values			Estimated Values		
	Wafer#2	Wafer#7	Wafer#11	Wafer#2	Wafer#7	Wafer#11
C_0	1.150e+2	1.267e+2	1.711e+2	8.072e+1	7.084e+1	1.228e+2
C_1	2.031e-1	7.004e-2	-1.994e+0	-1.695e+0	-2.266e+0	-4.318e+0
C_2	-4.278e+0	-5.466e+0	-4.162e+0	-7.427e+0	-9.370e+0	-8.747e+0
C_3	-2.302e-2	-2.831e-3	-2.978e-2	-6.572e-2	-4.064e-2	-9.004e-2
C_4	-3.945e-2	-5.695e-2	-7.789e-2	-8.089e-1	-1.958e+0	-2.826e+0
C_5	-3.639e+0	-5.320e+0	-6.246e+0	-1.616e-1	-2.882e-1	-1.698e-1
C_6	1.498e-2	5.297e-2	-2.247e-2	1.153e-1	2.524e-1	1.177e-1
C_7	-5.103e-2	1.388e+0	-1.043e+0	1.214e-2	1.733e-2	2.086e-2
C_8	4.148e-2	-2.645e+0	-2.190e+0	-2.660e-5	-4.373e-5	-4.280e-5
C_9	2.149d-2	5.339e-2	7.254e-2	2.092e-2	5.214e-2	7.362e-2
C_{10}	-2.367e-4	-2.999e-4	-2.334e-4	-1.282e-4	-2.808e-4	-1.319e-4
C_{11}	9.705e-2	1.053e-2	1.182e-2	1.232e-3	1.564e-3	2.067e-3
C_{12}	-4.054e-2	2.200e-2	-2.290e-2	-5.160e-4	-6.908e-4	-8.243e-4

Table 5.4: Calibrated Regression Coefficients for Primitive Variable Regression and Dimensional Analysis Models

5.4 Model Calibration and Analysis

The dimensional analysis model evolved in chapter 3 for the SN ratio (defined in equation 3.1) was regressed to the thickness mean and variance data . Instead of developing a single generalized SN ratio model for a batch, the data was utilized to develop a model for individual wafers located at different axial positions in the load. This approach did not require any extra effort in terms of experimentation or data acquisition. In fact, by doing so, the accuracy of the calibrated models was not degraded by the lack of fit for axial data that would otherwise be introduced if the axial

WAFER #	*Primitive Variables Model*		*Dimensional Analysis Model*	
	F-Test	Av. %Error	F-Test	Av. %Error
2	4.1	5.8	27.9	2.4
3	3.8	6.4	48.0	2.0
4	4.2	6.2	35.0	2.1
5	4.1	7.1	41.7	2.6
6	5.3	6.6	49.6	2.1
7	5.7	6.5	47.3	2.0
8	5.5	6.1	19.7	3.2
9	5.8	6.5	45.3	2.3
10	6.8	5.7	37.6	2.5
11	7.8	5.7	46.8	2.5

Table 5.5: F-Test & Average %Error Comparison of Primitive Model vs. Dimensional Model

dependence was considered. Therefore, coefficients C_0, C_1, ..., and C_{12} in equation 3.12 were determined for SN models for all test wafers in each run by multiple linear regression. The calibrated values of these coefficients for test wafers #2, #7, and #11 (see Fig.4.1) are given in Table 5.4.

For the same sets of data points, the SN model in equation 3.13 was calibrated. The calibrated values for the regression coefficients are given in Table 5.4.

Table 5.5 deals with the comparative analysis of the models in equation 3.12 and 3.13. It is very clear that the semi-empirical model based on dimensional analysis is much superior than the corresponding primitive variables model. The former has a much

lower average %error[1] and a F-ratio[2] that is six to seven times better than the latter.

The accuracy and better predictive power of the semi-empirical models is further demonstrated by predicting SN ratios for the individual wafers for certain sets of process parameters. These

TESTING CONDITIONS		Wafer #	SN obser -ved	SN predicted, Primitive	SN predicted, Dimensional
Run #	Process Parameters				
1.	w = .75 cm; r_h = .125 cm; T_d = 853. K; P = 375. mtorr; l_x = 49.8 cm; Q_S = 288.3 sccm; Q_{b1} = 3.14sccm; Q_{b2} = 1.07sccm	2	28.4	29.2 +/- 7.6	30.6 +/- 2.2
		7	31.2	28.4 +/- 8.2	30.6 +/- 2.0
		11	32.6	30.8 +/- 8.6	34.1 +/- 2.6
2.	w = .75 cm; r_h = .125 cm; T_d = 853. K; P = 325. mtorr; l_x = 65.1 cm; Q_S = 350.2 sccm; Q_{b1} = .58 sccm; Q_{b2} = .26 sccm	2	44.5	47.4+/-11.4	47.5 +/- 4.1
		7	49.0	52.6+/-12.2	54.5 +/- 4.0
		11	----	65.6+/-13.0	66.8 +/- 5.0
3.	w = .75 cm; r_h = .125 cm; T_d = 853. K; P = 375. mtorr; l_x = 42.2 cm; Q_S = 264.2 sccm; Q_{b1} = 3.07sccm; Q_{b2} = 1.52sccm	2	29.0	31.4+/-13.4	30.6 +/- 2.6
		7	33.6	29.4+/-14.4	30.6 +/- 2.4
		12	30.2	26.0 +/- 8.6	29.4 +/- 4.1

Table 5.6: SN Ratios Observed vs Predicted by Primitive Regression, and Dimensional Analysis Models

results for selected wafers are shown in Table 5.6 (results do hold for all the wafers in a batch)[3]. The dimensional analysis model predicts as good as the primitive variables model but the predictions of dimensional analysis model are much more reliable because of their narrow confidence intervals. This high reliability of the dimensional analysis model stems from the incorporation of the process physics into the model.

---

[1] The average %error is defined as the average of the % absolute deviation of the predicted SN value from the observed value.

[2] The F-ratio is the ratio of the mean square regression of calibartion coefficients to the mean square error in the regression.

[3] Note that the SN ratio in Table 5.6 is for individual wafers in a batch and not the SN ratio as used in Taguchi's method before.

The semi-empirical models for individual wafers were used to predict the batch's (and not individual wafers's) SN ratios SN_{T1} and SN_{T2} for the confirmation runs and the validity of these predictions was compared to that of Taguchi's averaging method. The SN_{T1} from dimensional analysis models, called $(SN_{T1})_{d,\ model}$, was determined by back-calculating $(\sigma_{T,i}/\mu_{T,i})^2$ ratio for every i^{th} wafer from its dimensional analysis model. These ratios for all wafers in a batch were added and averaged and then expressed in a decibel scale (as in equation 2.2 for SN_{T1}) to give the value for $(SN_{T1})_{d,\ model}$. Similarly, the SN_{T1} from primitive variables models, called $(SN_{T1})_{p,model}$, was determined from the primitive variables models for individual wafers. The SN_{T2}'s were determined by regressing equations 3.12 and 3.13 respectively to the data values of SN_{T2} for 18 runs. This gave semi-empirical model equations for $(SN_{T2})_{d,\ model}$ (from dimensional analysis equation 3.12) and $(SN_{T2})_{p,\ model}$ (from primitive variables equation 3.13). These equations for $(SN_{T2})_{d,\ model}$ and $(SN_{T2})_{p,\ model}$ were used for predicting the SN_{T2} for the corresponding confirmation run conditions. All these predictions in comparison to those of Taguchi's averaging method are shown in Table 5.7.

SN Type	Process Parameters for confirmation Runs	SN Ratio Values for Confirmation Runs			
		observed	predicted, Taguchi's	predicted, Dimensional	predicted, Primitive
SN_{T1}	w = .75; r_h = .125; T_d = 853.; P = 325.; l_x = 65.; Q_s = 350.2; Q_{p1} = .58; Q_{p2} = .26	46.2	**49.4 +/- 3.0**	**47.2 +/- 3.7**	**42.4 +/- 10.2**
SN_{T2}	w = .75; r_h = .328; T_d = 853.; P = 375.; l_x = 53.5; Q_s = 405.9; Q_{p1} = 2.87; Q_{p2} = .79	32.2	**31.1 +/- 13.4**	**30.3 +/- 3.3**	**32.0 +/- 14.1**

Note: Units for Process Parameters are: $[w]=[r_h]=[l_x]=[cm.]$; $[T_d]=[^oK]$; $[P]=[mtorr]$; $[Q_s]=[Q_{p1}]=[Q_{p2}]=[sccm]$

Table 5.7: Model Predictions vs. Taguchi's Method Predictions for Confirmation Runs

Once again the predictions by dimensional analysis models are more reliable than those by primitive variable models because the former has a narrower confidence interval. Also, these model predictions are better than those by Taguchi's averaging method in terms of confidence interval for SN_{T2} and mean value for SN_{T1}. This improvement is accounted for by the fact that in evolving these semi-empirical models we have incorporated important process variable interactions that Taguchi's method tends to neglect.

6. CONCLUSIONS

The orthogonal array design of experiments for process and equipment optimization was combined with a semi-empirical modelling approach based on dimensional analysis. Typical constraints of a purely empirical approach were experienced while applying Taguchi's method. These constraints included the lack of access to the desired experimental environment, a general drawback in empirical approach, and the problem of process parameter interactions, a particular limitation to Taguchi's orthogonal array method. Taguchi's method worked well for the optimization of In-Situ Phosphorus Doped Polysilicon Process via LPCVD. However, its dependence on the assumption that the process under consideration is free of parameter interactions proved to be an inhibiting limitation for at least one of the responses studied i.e nominal-is-the-best signal-to-noise ratio SN_{T1} for film thickness uniformity across the wafer. As a solution to such problems of purely experimental approach it was recommended to evolve a semi-empirical model for the process under consideration. Dimensional analysis was used as a way of formulating such a model for the film thickness uniformity in the process under consideration.

Dimensional analysis was used to transform primitive variables that described the process under consideration into dimensionless groups. It was theorized that these dimensionless groups would enhance empirical modeling by infusing some physical or causal reality of the process into the model. Enhancement, as expected, occured on two fronts. Dimensional analysis reduced the number of primitive experimental variables from eight to seven and primitive process variables (of which only 8 were varied in the experiments) from twelve to seven. Secondly, dimensional analysis, as theorized, yielded dimensionless parameters that were physically more significant than the primitive variables. The average % error in dimensional analysis model was about a third of that in primitive

variables model. Also, from statistical point of view, the F-test for dimensional analysis model was, on the average, six to seven times better than that for the corresponding primitive variables model. The dimensional analysis models had a more accurate and reliable predictive power as measured by the fact that the confidence interval of its predictions for a certain set of process conditions was more than three times narrower than that for primitive variables model predictions. The semi-empirical model overcame the problem encountered by Taguchi's method with regards to the importance of the process parameter interactions that the later tends to neglect.

For future work it is recommended that the semi-empirical model be derived for a response corresponding to the $SN_{overall}$ defined before. Dimensional analysis, as demonstrated in this work, should be used to evolve a model for such overall system response. For this to happen it is essential that the desired cost coefficients be determined by studying the economics of semi-conductor manufacturing. Such a model should be used to design a D-optimal set of experiments for optimizing and, therefore, designing process and equipment for in-situ doped polysilicon LPCVD process. It is also recommended that the strength of the semi-empirical approach shown in this work should be tested against a purely mechanistic model for the same process. Such a comparison is expected to reinforce the validity of the point made in this work that semi-empirical approach is the optimal way of designing optimal processes and equipment from modelling point of view. The potential of such an approach to process modelling in Manufacturing is enormous.

Acknowledgements

The author would like to thank Dr. Emanuel Sachs, ne thesis supervisor, for his guidance, encouragement, intense discussion, and enthusiasm that made this research effort a learning experience and a worthwhile effort. The author would also like to extend appreciation to William Wehrle and Michele Storm, fellow research students, for their intelligent suggestions along the way. The support extended by BTU Engineering Corporation's research staff, especially Mr. Arthur Waugh, Mr. Randy Rhoades, Mr. Steven Lai , and Morris Simpson, in terms of access to the equipment is appreciated.

Special thanks go to the Defense Advanced Research Projects Agency under contract MDA972-88-K-0008 for the support of this project.

APPENDIX A: Data Tables and Plots

The data acquired for the film thickness and resistivity of all the wafers in each of the 18 runs is outlined below in Tables A.1(1) to A.1(18). The ANOVA analysis for these runs is shown in Tables A.2, A.3, A.4, and A.5. The data for confirmatin runs is shown in Table A.6.

In the data Tables A.1(1) to A.1(18) and Table A.6, "t" is the film thickness, "Std.Dev._t" is the % standard deviation in film thickness, "rho" refers to the resistivity of the film, and "Std.Dev._rho" is the estimated[1] % standard deviation of resistivity. Next to the data tables, the axial profiles of average film thickness and resistivity are shown for each run. The missing data in table A.6 is due to the fact that the availability of insufficient number of test wafers forced us to replace the test wafers in some of the slots in the load by the dummy wafers. Also, some of the test wafers turned out to be defective and, therefore, accounted for the missing data points.

[1] Standard deviation in resistivity is estimated by multiplying standard deviations of film thickness and sheet resistance.

data.run# 1

	t (Angstorm)	Std. Dev _t	rho ($10^{-4}\Omega$_cm)	Std.Dev._rho
1	3040.000	1.07%	8.852	0.021%
2	3462.500	0.54%	8.248	0.004%
3	3593.100	0.39%	8.681	0.004%
4	3691.600	0.32%	9.281	0.001%
5	3789.600	0.23%	10.077	0.002%
6	3914.500	0.21%	10.992	0.002%
7	4075.800	0.23%	12.293	0.001%
8	4296.300	0.36%	13.986	0.003%
9	4552.100	0.20%	16.297	0.002%
10	4736.800	0.16%	18.417	0.001%
11	4669.100	0.11%	16.790	0.001%
12	3856.100	0.59%	13.940	0.008%

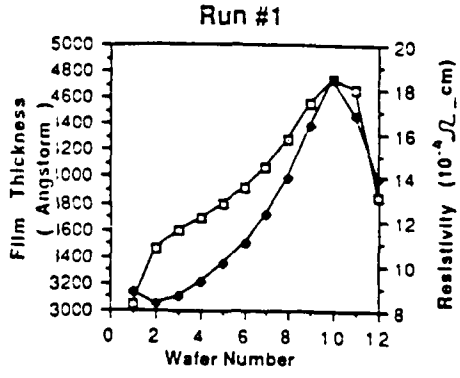

data.run#2

	t (Angstorm)	Std.Dev._t	rho ($10^{-4}\Omega$_cm)	Std.Dev._rho
1	2532.60000	4.87%	6.886	0.281%
2	2575.00000	2.85%	7.797	0.064%
3	2560.00000	2.60%	7.921	0.075%
4	2559.80000	2.91%	7.905	0.082%
5	2528.30000	2.57%	7.964	0.068%
6	2498.60000	2.26%	8.043	0.057%
7	2487.10000	2.32%	8.272	0.058%
8	2560.60000	2.20%	8.427	0.058%
9	2649.80000	1.55%	8.599	0.027%
10	2770.10000	1.59%	8.757	0.027%
11	2911.80000	1.36%	8.790	0.019%
12	2712.80000	2.33%	7.881	0.060%

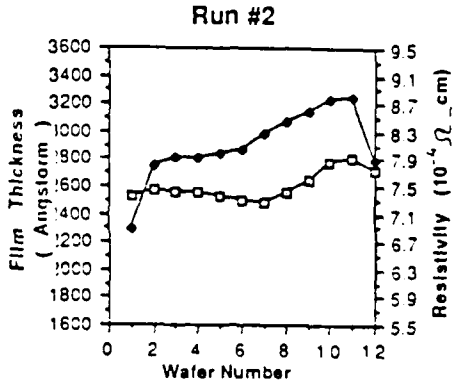

data.run#3

	t (A)	Std Dev _t	rho ($10^{-4}\Omega$_cm)	Std Dev _rho
1	3280.00000	7.72%	8.864	0.295%
2	2953.00000	5.59%	8.971	0.151%
3	2739.50000	4.96%	8.671	0.144%
4	2662.80000	5.71%	8.582	0.239%
5	2466.10000	5.51%	8.543	0.212%
6	2373.10000	5.20%	8.576	0.212%
7	2295.00000	4.68%	8.681	0.178%
8	2258.00000	3.55%	8.815	0.398%
9	2326.30000	3.95%	8.986	0.125%
10	2458.30000	4.91%	9.192	0.191%
11	2473.10000	3.90%	9.128	0.113%
12	2518.30000	6.63%	8.132	0.331%

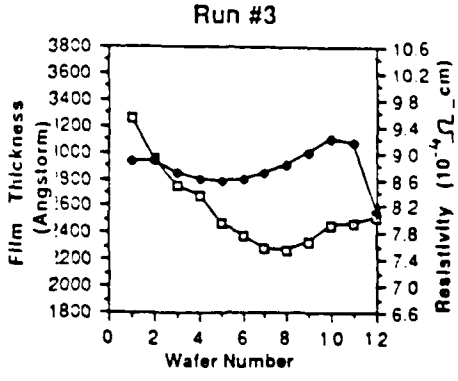

Table A.1(1)-(3): Data from Runs 1, 2, and 3

data.run#4

	t (Angstorm)	Std.Dev._t	rho ($10^{-4}\Omega$_cm)	Std.Dev._rho
1	1038.10000	7.20%	9.148	0.500%
2	1145.80000	5.04%	8.729	0.254%
3	1152.50000	5.49%	8.779	0.359%
4	1107.50000	5.38%	8.902	0.260%
5	1054.00000	5.92%	9.207	0.416%
6	1009.00000	6.05%	9.398	0.475%
7	970.16000	6.66%	9.528	0.545%
8	998.85000	7.09%	9.498	0.568%
9	997.56000	5.39%	9.644	0.335%
10	1021.90000	4.95%	9.536	0.284%
11	1009.00000	4.53%	9.510	0.242%
12	866.28000	5.91%	9.881	0.498%

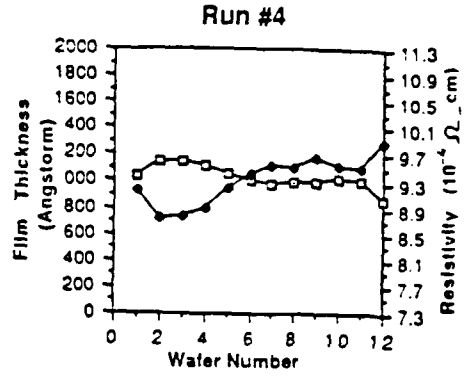

data.run#5

	t (Angstorm)	Std.Dev._t	rho ($10^{-4}\Omega$_cm)	Std.Dev._rho
1	5905.50000	2.10%	10.842	0.047%
2	6679.50000	1.19%	14.822	0.030%
3	6899.70000	0.83%	18.222	0.018%
4	7061.80000	0.87%	21.754	0.018%
5	7165.20000	0.50%	25.436	0.013%
6	7253.80000	0.56%	28.246	0.011%
7	7354.00000	0.82%	30.872	0.012%
8	7662.30000	0.82%	35.750	0.013%
9	8099.60000	0.38%	45.500	0.007%
10	8486.40000	0.25%	56.950	0.005%
11	8473.50000	0.16%	64.322	0.003%
12	7137.30000	0.51%	50.989	0.010%

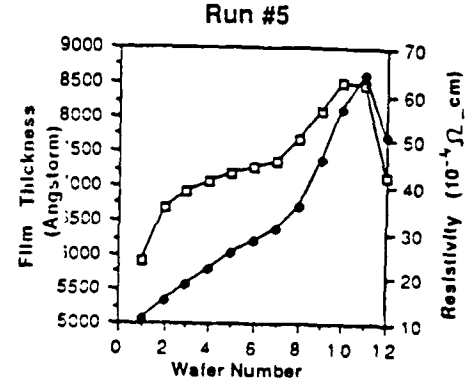

data.run#6

	t (Angstorm)	Std.Dev._t	rho ($10^{-4}\Omega$_cm)	Std Dev._rho
1	3612.60000	6.57%	11.250	0.227%
2	3810.30000	5.89%	10.989	0.184%
3	3670.80000	6.15%	10.491	0.238%
4	3498.60000	5.17%	10.191	0.168%
5	3376.80000	5.77%	10.012	0.216%
6	3281.80000	4.96%	9.885	0.171%
7	3262.30000	4.21%	9.790	0.139%
8	3324.10000	4.26%	9.909	0.154%
9	3418.60000	3.99%	10.297	0.109%
10	3561.60000	3.35%	10.671	0.104%
11	3593.60000	2.75%	11.129	0.060%
12	3264.60000	3.70%	10.698	0.118%

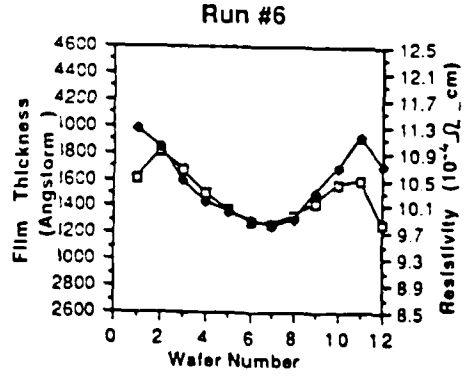

Table A.1(4)-(6): Data from Runs 4, 5, and 6

data.run#7

	t (Angstorm)	Std.Dev._t	rho ($10^{-4}\Omega$_cm)	Std.Dev._rho
1	2834.60000	5.27%	6.778	0.234%
2	2964.30000	5.76%	6.513	0.269%
3	2916.30000	4.03%	6.340	0.174%
4	2869.80000	4.16%	6.345	0.186%
5	2679.00000	4.07%	6.373	0.188%
6	2259.30000	7.60%	6.685	0.741%
7	1687.60000	7.62%	7.829	0.789%
8	1623.00000	6.95%	8.139	0.674%
9	1605.40000	4.96%	8.200	0.313%
10	1642.30000	4.28%	8.120	0.256%
11	1645.30000	3.58%	7.934	0.170%
12	1586.80000	3.29%	7.710	0.155%

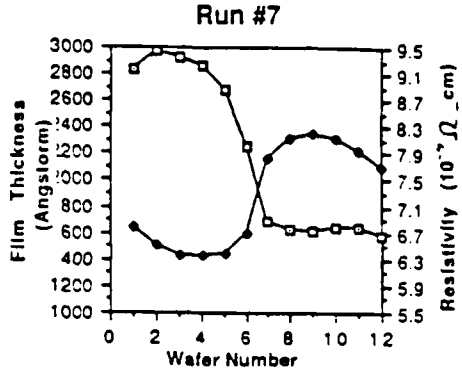

data.run#8

	t (Angstorm)	Std.Dev._t	rho ($10^{-4}\Omega$_cm)	Std.Dev._rho
1				
2	2860.80000	10.08%	7.355	1.166%
3	2928.30000	10.91%	7.190	1.215%
4	2478.80000	9.03%	7.474	0.891%
5	2369.80000	9.58%	7.515	1.073%
6	2285.30000	9.10%	7.679	1.007%
7	2203.30000	8.82%	7.667	0.837%
8	2247.30000	9.09%	7.843	1.054%
9	2250.30000	7.77%	7.858	0.715%
10	2248.10000	6.08%	7.913	0.474%
11	2293.30000	6.60%	8.003	0.548%
12	2054.00000	6.88%	8.025	0.595%

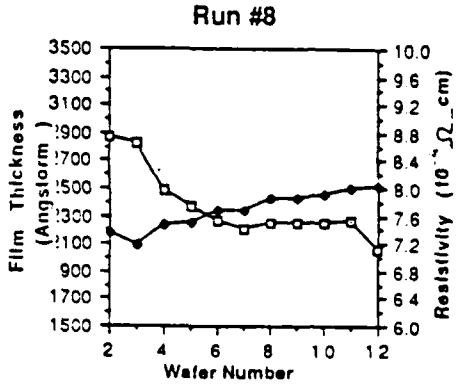

data.run#9

	t (Angstorm)	Std.Dev._t	rho ($10^{-4}\Omega$_cm)	Std.Dev._rho
1				
2	7875.60000	4.08%	17.444	0.108%
3	7671.10000	2.30%	18.886	0.032%
4	7420.20000	2.34%	19.678	0.047%
5	6813.00000	2.45%	18.872	0.044%
6	5975.10000	3.03%	16.581	0.046%
7	5291.70000	4.02%	14.753	0.072%
8	5099.80000	3.46%	14.642	0.063%
9	5298.10000	2.28%	15.863	0.038%
10	5590.70000	1.44%	17.532	0.027%
11	5762.60000	1.02%	18.942	0.019%
12	5217.00000	0.93%	18.912	0.014%

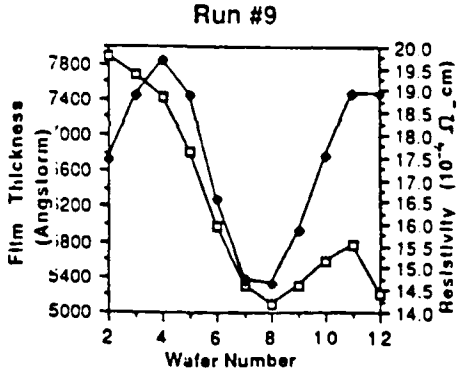

Table A.1(7)-(9): Data from Runs 7, 8, and 9

data.run#10

	t (Angstorm)	Std.Dev._t	rho ($10^{-4}\Omega$_cm)	Std.Dev._rho
1				
2	3599.60000	1.89%	9.553	0.010%
3	3676.60000	1.47%	8.975	0.010%
4	3742.00000	1.69%	8.782	0.006%
5	3823.80000	1.61%	8.818	0.022%
6	3887.60000	1.32%	8.805	0.016%
7	4032.00000	1.17%	8.834	0.018%
8	4200.50000	0.88%	8.817	0.012%
9	4367.10000	0.81%	8.760	0.012%
10	4531.50000	0.91%	8.755	0.014%
11	4476.30000	1.03%	8.950	0.016%
12	3855.50000	1.62%	9.018	0.024%

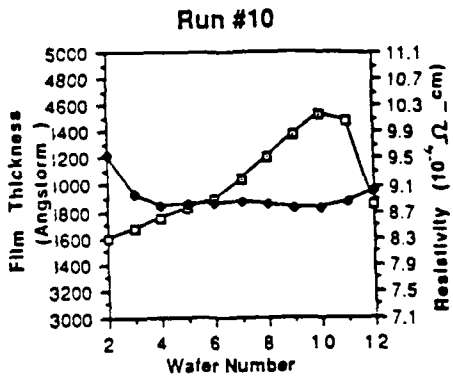

data.run#11

	t (Angstorm)	Std.Dev._t	rho ($10^{-4}\Omega$_cm)	Std.Dev._rho
1	3205.30000	7.35%	6.830	0.731%
2	2985.10000	4.73%	7.346	0.457%
3	2776.60000	4.12%	7.508	0.342%
4	2708.30000	3.38%	7.440	0.250%
5	2681.80000	4.13%	7.351	0.285%
6	2638.30000	4.08%	7.466	0.309%
7	2621.30000	3.83%	7.439	0.283%
8	2704.50000	3.00%	7.519	0.225%
9	2814.50000	2.69%	7.487	0.171%
10	2927.80000	2.69%	7.478	0.194%
11	2926.10000	3.24%	7.406	0.199%
12	2512.80000	3.51%	7.232	0.228%

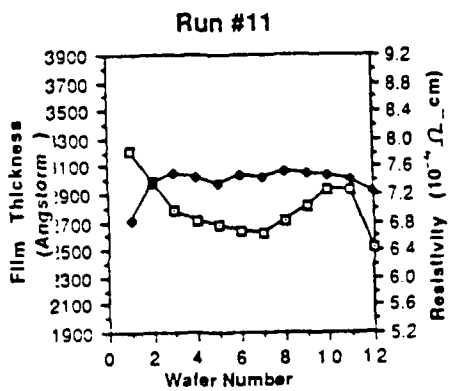

data.run#12

	t (Angstorm)	Std.Dev._t	rho ($10^{-4}\Omega$_cm)	Std.Dev._rho
1	6157.20000	3.06%	10.498	0.083%
2	6012.20000	2.79%	10.822	0.129%
3	5283.60000	2.60%	10.403	0.104%
4	4615.70000	3.27%	9.739	0.141%
5	4018.10000	3.39%	9.125	0.195%
6	3571.80000	3.36%	8.819	0.197%
7	3296.60000	3.61%	8.644	0.222%
8	3177.60000	3.38%	8.649	0.204%
9	3197.50000	3.04%	8.691	0.183%
10	3274.10000	3.06%	8.703	0.181%
11	3326.10000	2.72%	8.711	0.163%
12	3103.30000	4.41%	8.255	0.286%

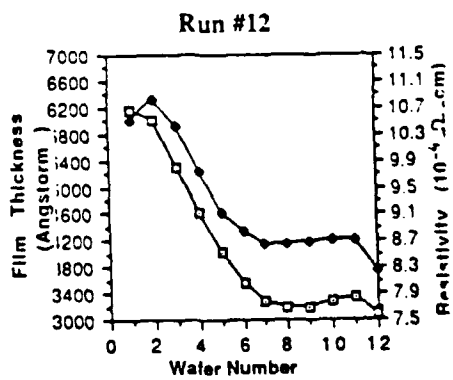

Table A.1(10)-(12): Data from Runs 10, 11, and 12

data.run#13

	t (Angstorm)	Std.Dev._t	rho ($10^{-4}\Omega$_cm)	Std.Dev._rho
1				
2	2290.60000	6.83%	7.570	0.390%
3	2219.80000	5.27%	6.968	0.386%
4	2168.10000	5.12%	7.111	0.463%
5	2103.60000	5.51%	7.264	0.564%
6	2029.10000	6.30%	7.331	0.607%
7	1975.10000	6.41%	7.385	0.575%
8	1996.40000	6.20%	7.341	0.409%
9	2072.60000	5.67%	7.486	0.460%
10	2159.80000	4.91%	7.469	0.406%
11	2166.10000	4.40%	7.412	0.268%
12	1812.30000	6.16%	7.610	0.499%

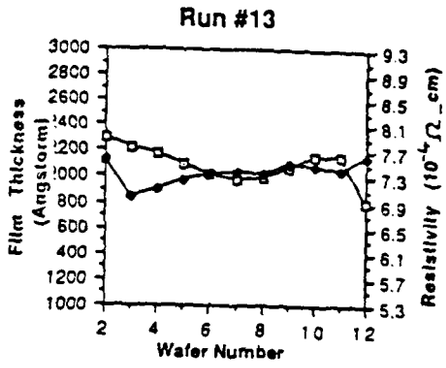

data.run#14

	t (Angstorm)	Std.Dev._t	rho ($10^{-4}\Omega$_cm)	Std.Dev._rho
1	6769.10000	3.13%	8.698	0.105%
2	7129.80000	4.74%	6.887	0.152%
3	6530.30000	4.40%	6.191	0.228%
4	5454.10000	4.94%	6.185	0.374%
5	4534.70000	5.39%	6.725	0.379%
6	3867.80000	5.80%	6.923	0.453%
7	3470.60000	6.13%	7.236	0.409%
8	3436.30000	5.58%	7.471	0.488%
9	3548.60000	5.03%	7.519	0.426%
10	3678.10000	4.99%	7.507	0.409%
11	3648.10000	4.45%	7.446	0.290%
12	3180.30000	5.33%	6.895	0.324%

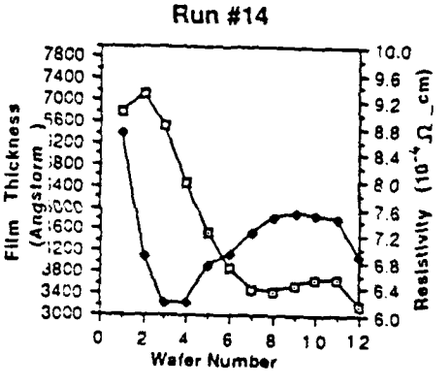

data.run#15

	t (Angstorm)	Std.Dev._t	rho ($10^{-4}\Omega$_cm)	Std.Dev._rho
1	6176.20000	5.38%	8.400	0.406%
2	6885.70000	5.72%	9.275	0.355%
3	6547.00000	4.43%	9.519	0.283%
4	6328.80000	4.86%	9.651	0.215%
5	6205.00000	4.85%	10.164	0.282%
6	6134.00000	4.11%	10.722	0.230%
7	6213.80000	3.84%	11.564	0.218%
8	6398.20000	3.37%	12.310	0.173%
9	6647.30000	3.25%	13.168	0.147%
10	6787.20000	2.85%	13.927	0.120%
11	6737.00000	2.30%	14.451	0.098%
12	5701.30000	2.73%	13.535	0.103%

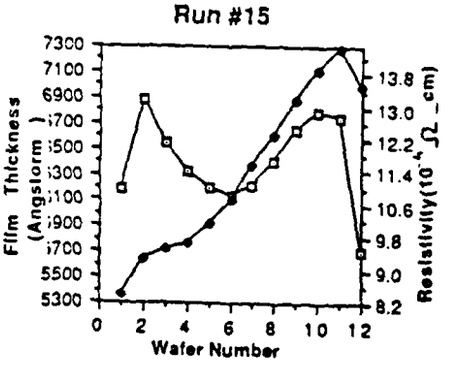

Table A.1(13)-(15): Data from Runs 13, 14, and 15

data.run#16

	t (Angstorm)	Std.Dev._t	rho ($10^{-4}\Omega$_cm)	Std.Dev._rho
1	4617.00000	3.07%	9.049	0.054%
2	5257.10000	3.03%	8.522	0.073%
3	5332.70000	2.58%	8.591	0.061%
4	5284.80000	2.49%	8.588	0.033%
5	5165.20000	2.77%	8.585	0.042%
6	4980.00000	2.89%	8.322	0.039%
7	4853.50000	3.55%	8.023	0.052%
8	4926.20000	2.91%	7.936	0.040%
9	5115.10000	2.31%	8.123	0.027%
10	5254.70000	1.71%	8.423	0.014%
11	5217.10000	1.89%	8.786	0.027%
12	4483.20000	2.25%	8.307	0.044%

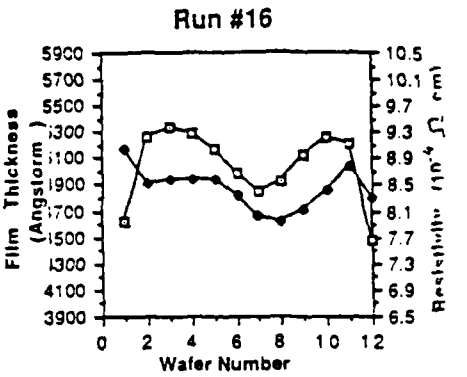

data.run#17

	t (Angstorm)	Std.Dev._t	rho ($10^{-4}\Omega$_cm)	Std.Dev._rho
1	4907.20000	9.81%	5.864	1.081%
2	5059.80000	9.98%	5.905	1.421%
3	4331.00000	7.07%	6.263	0.949%
4	3891.80000	6.83%	6.674	0.644%
5	3499.30000	6.82%	7.072	0.658%
6	3229.80000	7.31%	7.180	0.805%
7	2983.60000	8.03%	7.507	1.013%
8	2952.50000	8.05%	7.538	1.000%
9	2979.00000	6.71%	7.471	0.703%
10	3036.30000	6.46%	7.339	0.439%
11	3003.80000	6.18%	7.488	0.590%
12	2559.60000	6.93%	7.643	0.716%

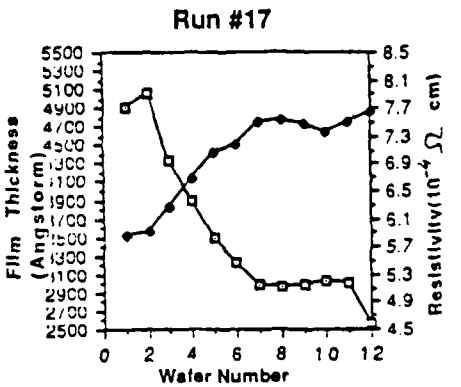

data.run#18

	t (Angstorm)	Std.Dev._t	rho ($10^{-4}\Omega$_cm)	Std.Dev._rho
1	5251.70000	8.01%	6.843	0.812%
2	5756.70000	8.92%	7.035	1.237%
3	5347.30000	8.40%	6.914	1.110%
4	5016.20000	8.36%	6.907	1.172%
5	4876.50000	8.50%	6.915	1.153%
6	4746.10000	8.61%	7.005	1.178%
7	4632.20000	8.47%	7.171	1.017%
8	4755.20000	9.59%	7.442	1.401%
9	4822.70000	7.55%	7.321	0.866%
10	4846.80000	7.02%	7.333	0.696%
11	4830.20000	6.85%	7.385	0.709%
12	4190.00000	7.25%	7.253	0.753%

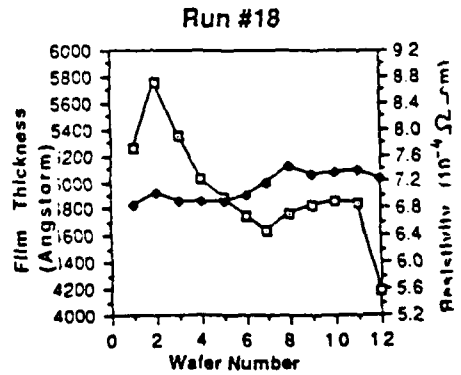

Table A.1(16)-(18): Data from Runs 16, 17, and 18

Factor	Degrees of Freedom	Sum of Squares	Mean Sum of Squares	F-Ratio	% Effect	Rank
w	1	35.422	35.422	39.508	4.5%	5
A_c	2	176.405	88.202	98.377	22.2%	2
T	2	72.430	36.215	40.393	9.1%	4
P	2	14.944	7.472	8.334	1.9%	7
I_x	2	29.563	14.782	16.487	3.7%	6
Q_s	2	5.619	2.809	3.133	0.7%	8
Q_{b1}	2	309.799	154.899	172.768	38.9%	1
Q_{b2}	2	149.514	74.757	83.381	18.8%	3
Error	2	1.793	0.897			
Total	17	795.487				

Table A.2: ANOVA for SN_{T1}

Factor	Degrees of Freedom	Sum of Squares	Mean Sum of Squares	F-Ratio	% Effect	Rank
w	1	.789	.789	0.036	0.19%	8
A_c	2	38.399	19.199	0.885	9.40%	3
T	2	8.092	4.046	0.187	1.97%	6
P	2	2.498	1.249	0.058	0.61%	7
I_x	2	35.763	17.882	0.824	8.70%	4
Q_s	2	22.296	11.148	0.514	5.40%	5
Q_{b1}	2	39.240	19.620	0.904	9.60%	2
Q_{b2}	2	219.856	109.928	5.070	53.6%	1
Error	2	43.391	21.696			
Total	17	410.323				

Table A.3: ANOVA for SN_{T2}

Factor	Degrees of Freedom	Sum of Squares	Mean Sum of Squares	F-Ratio	% Effect	Rank
w	1	6.040	6.040	35.483	8.0%	4
A_c	2	1.151	0.576	6.761	1.5%	7
T	2	13.553	6.777	79.625	18.0%	3
P	2	0.068	0.034	0.398	0.1%	8
I_x	2	3.189	1.595	18.737	4.2%	5
Q_s	2	2.886	1.443	16.953	3.8%	6
Q_{b1}	2	32.609	16.304	191.577	43.4%	1
Q_{b2}	2	15.343	7.671	90.139	20.4%	2
Error	2	0.340	0.170			
Total	17	75.178				

Table A.4: ANOVA for SN_G

Factor	Degrees of Freedom	Sum of Squares	Mean Sum of Squares	F-Ratio	% Effect	Rank
w	1	38.334	38.334	6.019	17.3%	2
A_c	2	20.305	10.152	1.594	9.2%	5
T	2	5.682	2.841	0.446	2.6%	8
P	2	10.742	5.371	0.843	4.8%	7
I_x	2	27.982	13.991	2.197	12.6%	4
Q_s	2	11.352	5.676	0.891	5.1%	6
Q_{b1}	2	61.881	30.941	4.858	27.9%	1
Q_{b2}	2	32.799	16.400	2.575	14.8%	3
Error	2	12.739	6.369			
Total	17	221.816				

Table A.5: ANOVA for SN_P

Data Conf.Run#1.SNt1

	t (Angstorm)	Std. Dev._t
1	4952.200000	0.787%
2	4440.500000	0.954%
3	4396.100000	0.334%
4		
5	4463.000000	0.386%
6		
7	4589.000000	0.361%
8		
9	4877.300000	0.223%
10		
11		
12	3983.500000	0.397%

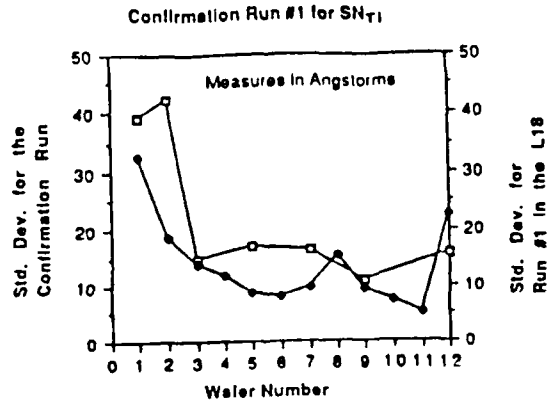

Data Conf.Run#2.SNt2

	t (Angstorm)	Std. Dev._t
1		
2		
3	2921.300000	1.797%
4		
5		
6		
7		
8		
9	3172.100000	1.398%
10		
11	3264.100000	0.733%
12	3855.100000	0.561%

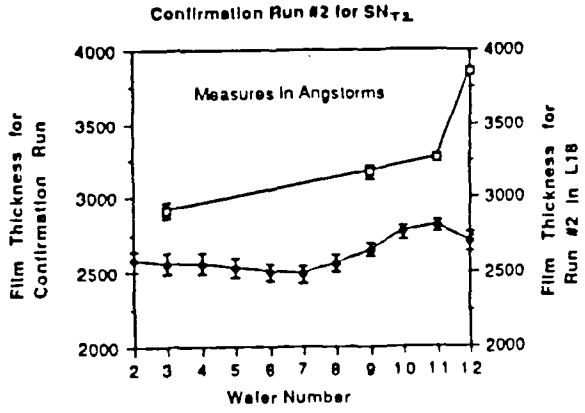

Data Conf.Run#3 SNg

	t (Angstorm)	Std. Dev._t
1		
2	5139.500000	4.661%
3		
4		
5		
6	5703.500000	1.363%
7		
8		
9		
10		
11	6518.700000	0.910%

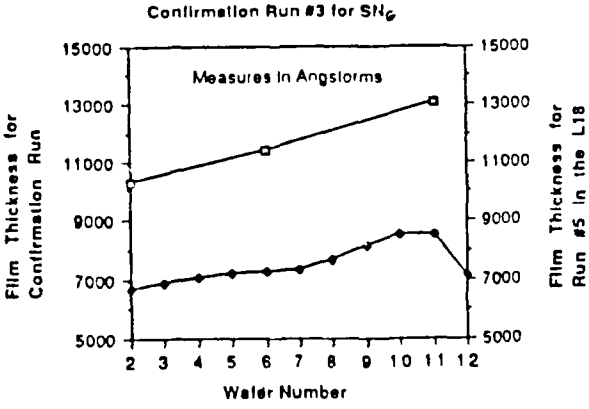

Data Conf.Run#4 SNr

	rho (10^{-4} ohm-cm)
1	
2	12.330669
3	12.710015
4	
5	12.861547
6	
7	13.070076
8	
9	12.577869
10	
11	12.239946
12	13.490182

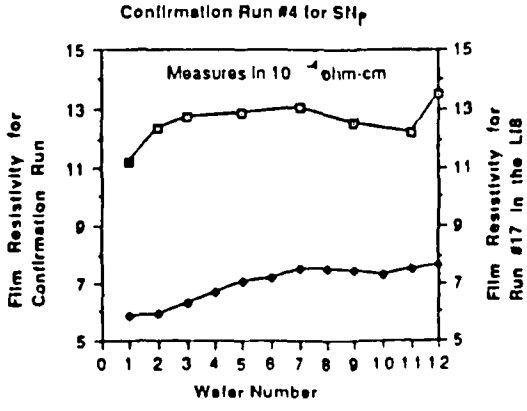

Table A.6: Data for the Confirmation Runs

APPENDIX B: Cost Function Derivations

(1) Film Thickness Quality Loss:

There are two kinds of film thickness quality loss functions, across-the-wafer thickness variance cost, and the cost due to the total variance across a batch (across-the-wafer "plus" down-the-load):

(a) Quality Cost due to Across-the-wafer Variance:

Each batch consists of n_w wafers with "$\mu_{T,i}$" and "$\sigma_{T,i}$" as the mean and standard deviation of the film thickness of the ith wafer. Quality loss due to ith wafer in a batch is the sum of the squared deviation of the average value of wafer film thickness from target $\mu_{T,t}$ and the resulting mean squared deviation of film thickness around its own mean.

$$Q_i = k_{T1}\left(\sigma_{T,i}^2 + (\mu_{T,i} - \mu_{T,t})^2\right) \qquad \text{(B.1)}$$

where k_{T1} is the corresponding quality loss coefficient that converts the loss into a $ value. Now if a adjustment factor like deposition time is increased by a factor $(\mu_{T,t}/\mu_{T,i})$ so as to obtain the target thickness, the corresponding standard deviation after adjusting the mean changes to $(\mu_{T,t}/\mu_{T,i})\sigma_{T,i}$ and the adjusted quality loss for a wafer is given by

$$Q_i^a = k_{T1}\mu_{T,t}^2\left(\frac{\sigma_{T,i}}{\mu_{T,i}}\right)^2 \qquad \text{(B.2)}$$

The total adjusted quality loss for a batch, as defined by Taguchi, can be expressed in two ways. Firstly, the sum of losses incurred by individual wafers (Equation B.2) can be used to represent the total average loss for a batch. Note that this loss is only due to the thickness variance across the wafers and is given by

$$QL_{T1} = k_{T1}\,\mu_{T,i}^2\left[\frac{1}{n_w}\sum_{i=1}^{n_w}\left(\frac{\sigma_{T,i}^2}{\mu_{T,i}^2}\right)\right] \qquad (B.3)$$

In Equation B.3 it is assumed that the quality loss coefficient k_{T1} is same for all wafers in a batch. This is justified because in case a batch has to be scrapped, all the wafers have same dollar expense inccured in them.

(b) Quality Cost due to Total Batch Variance:

Once again, considering that each batch consists of n_w wafers with "$\mu_{T,i}$" and "$\sigma_{T,i}$" as the mean and standard deviation of the film thickness of the ith wafer, the overall mean for the batch is given by

$$\mu_T = \frac{1}{n_w}\sum_{i=1}^{n_w}\mu_{T,i} \qquad (B.4)$$

If the thickness variance of the ith wafer is based on m_i data points across a wafer then the batch variance is given by

$$\sigma_T^2 = \frac{\sum_{i=1}^{n_w}\left(\sigma_{T,i}^2 + \mu_{T,i}^2\right)m_i}{\sum_{i=1}^{n_w} m_i} - \mu_T^2 \qquad (B.5)$$

In equation B.5 the variance across the wafer $\sigma_{T,i}$ is "added" to the variance of the mean $\mu_{T,i}$ down the load. If the variance of all wafers is based on same number of data points then

$$\sigma_T^2 = \frac{1}{n_w}\sum_{i=1}^{n_w}\left(\sigma_{T,i}^2 + \mu_{T,i}^2\right) - \mu_T^2 \qquad (B.6)$$

Therefore, the total batch variance incorporating down-the-load variance as well as across-the-wafer.variance is given by,

$$QL_{T2} = k_{T2}\,\mu_{T,t}^2\left(\frac{\sigma_T^2}{\mu_T^2}\right) \qquad (B.7)$$

where k_{T2} is the loss coefficient for total variance in a batch.

For a target film thickness of $\mu_{T,t}$ (A^o) consider A_o as the \$ cost incurred in discarding a batch if across-the-wafer nonuniformity exceeds a functional limit of Δ_{T1} (A^o). Using this in Equation B.4, we get ,

$$k_{T1} = \frac{A_o}{\Delta_{T1}^2}\left[\frac{\$}{(A^o)^2}\right] \qquad (B.8)$$

Similarly, imposing the functional limit of Δ_{T2} (A^o) on total thickness variation in batch (across-the-wafer "plus" down-the-load), we get,

$$k_{T2} = \frac{A_o}{\Delta_{T2}^2}\left[\frac{\$}{(A^o)^2}\right] \qquad (B.9)$$

(2) Growth Rate Loss:

Growth rate degradation is not a quality loss because to compensate for lower growth rate one can increase the deposition time without scrapping the lot. Therefore, the loss incurred due to increased deposition time is only the increased total labor, equipment, and floor space costs C_L, C_E, C_F (\$) respectively. For a wafer, this cost falls as the average growth rate for a wafer rises. Again, summing the individual wafer costs, we get the average batch cost for lower growth rates as,

$$C_G = k_G\,\mu_{T,t}\left[t_o\,\frac{1}{n_w}\sum_{i=1}^{n_w}\left(\frac{1}{\mu_i}\right)\right] \qquad (B.10)$$

where k_G is the loss coefficient that expresses the above loss in \$ value. Consider a fixed cost rate c_L, c_E, and c_F (\$/min) for labor, equipment, and floor space respectively. The total cost incurred for deposition time t_o is

$$C_G = (t_o + t_1)(c_L + c_E + c_F) \qquad \text{(B.11)}$$

where t_1 is the fixed time for predeposition and postdeposition steps. If the deposition time t_o is increased to t_o^* then the film thickness achieves the target $\mu_{T,t}$. Using this fact in Equation B.11 and after readjustment, we get,

$$k_G = (c_L + c_F + c_E)\left(1 + \frac{t_1}{t_o^*}\right) \left[\frac{\$}{\text{min}}\right] \qquad \text{(B.12)}$$

(3) Film Resistivity Quality Loss:

The target is to minimize the resistivity of the film. For zero quality loss the desired resistivity is zero. However, physically it is impossible to obtain zero resistivity. Therefore, any value of resistivity leads to some loss. Modelling this loss as a quadratic loss, we get the average loss for a batch as

$$QL_\rho = k_\rho \left[\frac{1}{n_w}\sum_{i=1}^{n_w} \mu_{\rho_i}^2\right] \qquad \text{(B.13)}$$

where k_ρ is the resistivity quadratic loss coefficient. Now consider that the batch is scrapped at a loss of A_o (\$) if the average film resistivity in a batch exceeds the functional limit of Δ_ρ above the target of μ_ρ Ω_cm (which is zero ideally). Using these facts in equation B.13, we get,

$$k_\rho = \frac{A_o}{\Delta_\rho^2} \left[\frac{\$}{(\Omega\text{\_cm})^2}\right] \qquad \text{(B.14)}$$

References

[1] K.F. Jensen and D.B. Graves; *"Model and Analysis of Low Pressure CVD Reactors"* ; Journal of Electrochemical Society, vol. 130, no. 9, pp 1950-1957, 1983.

[2] K.F. Roenigk and K.F. Jensen; *" Analysis of Multicomponent LPCVD Processes"* ; Journal of Electrochemical Society, vol. 132, no. 2, pp 448-454, 1985.

[3] S. Middleman and A. Yeckel; *"A Model of the Effects of Diffusion and Convection on the Rate and Uniformity of Deposition in CVD Reactor"* ; Journal of Electrochemical Society, vol. 133, no. 2, pp 1051-1056, 1986.

[4] B.S. Meyerson and W. Olbricht; *"Phosphorus-Doped Polycrystalline Silicon via LPCVD I"* ; Journal of Electrochemical Society, vol. 131, no. 10, pp 2361-2365, Oct. 1984.

[5] B.S. Meyerson and M.L. Yu; *"Phosphorus-Doped Polycrystalline Silicon via LPCVD II"* ; Journal of Electrochemical Society, vol. 131, no. 10, pp 2366-2368, Oct. 1984.

[6] Gunther Harbeke, Liselotte Krausbauer, Edgar F. Steigmeier, Alois E. Widmer, Heinz F. Kappert and Gerd Neugebauer; *"LPCVD Polycrystalline Silicon: Growth and Physical Properties of In-Situ Phosphorus Doped and Undoped Films"* ; RCA Review, vol. 44, pp 287-312, June 1983.

[7] M.T. Duffy, J.T. McGinn, J.M. Shaw, R.J. Smith, R.A. Soltis and G. Harbeke; *"LPCVD Polycrystalline Silicon: Growth and Physical Properties of Diffusion-Doped, Ion-Implanted, and Undoped Films"* ; RCA Review, vol. 44, pp 313-325, June 1983.

[8] D.W. Foster and A.J. Learn; *"An In-Situ Phosphorus Doped Polysilicon Deposition Process Optimized for Production"* ; Proc. 3rd Int. VLSI Multilevel Interconnection Conf. (IEEE, New York, NY, 1986), pp 523.

[9] Arthur J. Learn and Derrick W. Foster; *"Deposition and Electrical Properties of in-situ Phosphorus-Doped Silicon films formed by Low Pressure Chemical Vapor Deposition"* ; Journal of Applied Physics, vol. 61, no. 5, pp1898-1904, March 1987.

[10] F.C. Eversteyn and B.H. Put; *"Influence of AsH_3, PH_3, and B_2H_6 on the Growth Rate and Resistivity of Polycrystalline Silicon Films Deposited from a SiH_4-H_2 Mixture"* ; Journal of Electrochemical Society, vol. 120, no. 1, pp 106-110, Jan. 1973.

[11] M.L. Hitchman, J. Kane and A.E. Widmer; *"Polycrystalline Growth Kinetics in a Low Pressure Chemical Vapor Deposition Reactor"* ; Thin Solid Films, vol. 59, pp 231-247, 1979.

[12] W.A. Bryant; *"The Kinetics of the Deposition of Silicon by Silane Pyrolysis @ Low Temperature and Atmospheric Pressure"* ; Thin Solid Films, vol. 60, pp 19-25, 1979.

[13] M.S. Phadke, R.N. Kacker, D.V. Speeney and M.J. Grieco; *"Off-Line Quality Control in Integrated Circuit Fabrication Using Experimental Design"* ; The Bell System Technical Journal, vol. 62, no. 5, pp 1273-1309, 1983.

[14] Ramon V. Leon, Anne C. Shoemaker and Raghu N. Kacker; *"Performance Measures Independent of Adjustment"*; Technometrics, vol. 29, no. 3, pp 253-285, Aug. 1987.

[15] G. Taguchi; *Introduction to Quality Engineering* ; Tokyo: Asian Productivity Organization, 1986.

[16] G.E.P. Box, W.G. Hunter and J.S. Hunter; *Statistics for Experimenters* ; John Wiley & Sons, 1978.

[17] Madhav S. Phadke; *Quality Engineering Using Robust Design* ; Prentice Hall, Inc.

[18] K.J. Laidler; *Chemical Kinetics* ; McGraw Hil Book Co., 1965.

[19] C.G. Hill; *Chemical Engineering Kinetics and Reactor Design.*